

## Chapter 5

# Data Wrangling *Analysis*

The work discussed in this chapter was done in close collaboration with Dr. Ralf Seidl, Dr. Francesca Giordano, Daniel Jumper, and Abraham Meles. Eventually the analysis group merged with another year's analysis group, bringing in Dr. Sanghwa Park, and Dr. Chong Kim, who have made crucial contributions to this analysis, and have studied the complimentary 2012 data set, producing their own PhD theses on this analysis. Dr. Hideyuki Oide has also heavily influenced the techniques and work-flow of this analysis, pioneering many of the techniques used here (at PHENIX at least) for his analysis of the 2011 data set.

*so who died  
you add?  
It's your thesis  
don't give credit  
etc...*

### 5.1 Overview

Although we have discussed in detail the theoretical motivations for the W physics program, as well as the machines producing the necessary collisions and recording data produced from these collisions, we have not yet addressed the form of the data set itself, and the substantial engineering it takes to extract the signal of interest out of that data set.

The relative abundance of the  $p + p \rightarrow W^\pm \rightarrow \mu^\pm + \nu$  signal events is rather low, compared to the other interactions which may take place when two protons collide. We must allow several hundred million proton proton collisions to occur, before we have a high probability of observing just one W-Boson event.

We discussed in the previous chapter how careful triggering is employed in order to ensure that any time this event does occur, it is recorded. This does not guarantee that we *only* record these events. Background events are still recorded much more frequently than

# DRAFT

The each physics trigger is conveniently stored as a 32-bit integer. This is a very special integer, because it does not take on all possible values that a 32-bit integer can take on. A trigger with a bitnumber of '2' means that the second binary digit of the trigger's binary representation is flipped to "1" and the rest of the digits are "0". In this way, one can easily store and check which triggers for a recorded event actually fired. Thus, an important variable called 'trigscaled' in this analysis can be created, to track which triggers which fired on a certain event by taking the bitwise-OR operation between all binary representations of triggers which fired for that event.

For example, consider a simplified version of this scheme with four assigned trigger bits. Let's say we have an event where the following triggers fired:

For example

- Trigger 1 Fired: 0001
- Trigger 3 Fired: 0100
- Trigger 4 Fired: 1000

The boolean-OR bitwise comparison is then:

- Trigscaled: 1101

Note how we lost no information regarding which triggers fired for this event. We can recover later, in code, the trigger mix for every event by using bitwise-AND operations, so long as we know which triggers were assigned to which bit, and we have the trig-scaled number.

This bit-masked final number, ones and zeroes, is one of the crucial variables in all PHENIX data sets (discussed in the next chapter). It is crucial to know which triggers fired for which event so that the original collision conditions, and therefore the physics, can be reconstructed. Since each detector subsystem may not have the same geometric acceptance, trigger acceptance, signal ~~traducing~~ hardware, triggering, while necessary for taking data, introduces severe bias into the data set. Knowledge of which triggers fire for each recorded event gives us the ability to correct for these kinds of biases to recover the original conditions of the data sample.

# DRAFT

Name	Scale Down	Raw Trigger Rate	Livetime
BBCLL1(>0 tubes)	31141	1921013.65	0.89
BBCLL1(>0 tubes) novertex	6732	3196505.83	0.89
ZDCLL1wide	6227	370696.78	0.9
BBCLL1(noVtx)&(ZDCN  ZDCS)	6396	1498978.93	0.9
BBCLL1(>0 tubes) narrowvtx	4070	925279.35	0.89
ZDCNS	4411	233334.89	0.89
ERT_4x4b	0	93.22	0.88
ERTLL1_4x4a&BBCLL1(noVtx)	0	490.47	0.89
ERT_4x4c&BBCLL1(noVtx)	1	2191.87	0.9
SG3&MUID_1H_N  S	95	14830.21	0.88
ERTLL1_E&BBCLL1(narrow)	1	1039	0.9
CLOCK	46765	9388833.68	0.89
MPC_B	0	263.11	0.89
MPC_A	0	1511.4	0.89
MPC_C&ERT_2x2	0	189.37	0.9
(MPCS_C&MPCS_C)  ((MPCN_C&MPCN_C)	0	10.19	0.63
((MUIDLL1_N2D  S2D)  ((N1D&S1D))&BBCLL1(noVtx)	0	260.64	0.63
(MUIDLL1_N1D  S1D)&BBCLL1(noVtx)	55	20196.39	0.87
RPC1+RPC3_S	359	23841.89	0.9
RPC1+RPC3_N	539	72270.55	0.9
SG3&RPC3&MUID_1D_N  S	2	5526.47	0.86
SG1+RPC1(C)&MUIDLL1_N  S	0	146.32	0.86
MUON_S.SG1_RPC3A&MUID_S1D	0	31.27	0.89
MUON_N.SG1_RPC3A&MUID_N1D	0	74	0.84
MUON_S.SG1&BBCLL1(noVtx)	2697	323237.99	0.9
MUON_N.SG1&BBCLL1(noVtx)	11128	1095764.77	0.9
MUON_S.SG1_RPC3_1_B  C	0	66.32	0.89
MUON_N.SG1_RPC3_1_B  C	0	173.57	0.88

Table 4.4: A typical run from the 2013 data set. This run was numbered '396418', according to PHENIX's numbering scheme. The 'name' column is the name given to the physics trigger, with one trigger per row. Names are descriptive, such that when boolean operators appear, this corresponds to that operation on the presence of that particular subsystem's trigger signal. Though a W-boson can occur for any triggered events, events firing a 'MUON' styled trigger are most likely. One can get a flavor for the relative frequency of triggers in the "Raw Trigger Rate" column (Hz), as well as the relative importance of that trigger in data taking, from the "Scale Down" column. Rare triggers have a smaller scale-down than common ones. The live-time column describes the fraction of the time that PHENIX saw an event worthy of recording, and then recorded it.

too much  
 I make  
 a text not  
 caption

# DRAFT

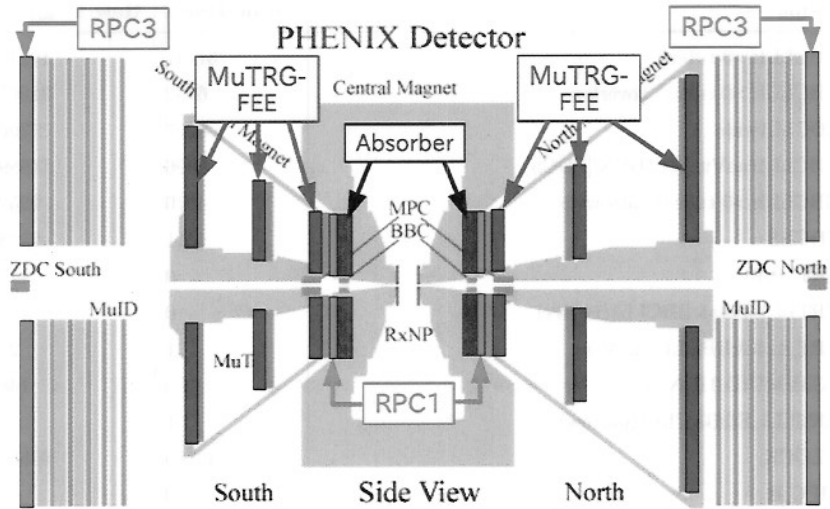


Figure 4.33: The position of the Front-End Electronics upgrades and new RPCs + Absorber are shown. Muon tracker stations are shown in blue (along with the front-end electronics). The RPCs sandwich the muon tracking stations and the MuID. The absorber material sits just inside of the muon arms, before the Forward Vertex Detectors and inner tracking stations of the muon tracker [64]

*Yes and no  
need to record neutrals, and its prescale, and prescale at my trigger...  
not to archive the data which is produced.*

The over all trigger rates must be recorded, so as to reconstruct the relative abundance of events after the fact. Once a trigger condition has been satisfied, the entire PHENIX spectrometer will dump its data into the data stream.

The PHENIX DAQ can accommodate 32 different physics triggers. Any transduced signal by a part of the PHENIX spectrometer can be, provided the front end electronics are fast enough, be fed into a global triggering decision. Thus, PHENIX, like other triggered particle physics experiments can be arbitrarily configured to record a desired subset of data, from the total data set.

Of the 32 triggers available, one is always set to 'Noise' (but not recorded) and another is set to 'CLOCK' which is timed to trigger every beam crossing. No bandwidth is reserved for these triggers. There was one global physics trigger configuration used in the Run 13 data set, it was called 'PP510Run13'. An example configuration is shown in Table ??.

*known as*

*If no bandwidth why do you mention it?*

82

*If there's ONE  
why is this an  
"example" it is  
or it is not.*

# DRAFT

### 4.5.3 Triggering and Data Acquisition

The new triggering scheme incorporating the RPCs and the new FEEs is summarized in Figure 4.32, while the final configuration of the PHENIX detector after the forward upgrade is show in Figure 4.33. As discussed, data was recorded at about 30% of the total PHENIX DAQ bandwidth of 8 kHz over the 2013 polarized proton+proton run, which was sufficient to record every single  $W \rightarrow \mu$  event. This speaks to the relative rarity of this event, as compared to other events - the overall collision rate for protons at  $510\text{GeV}/c^2$  is as high as 10 MHz.

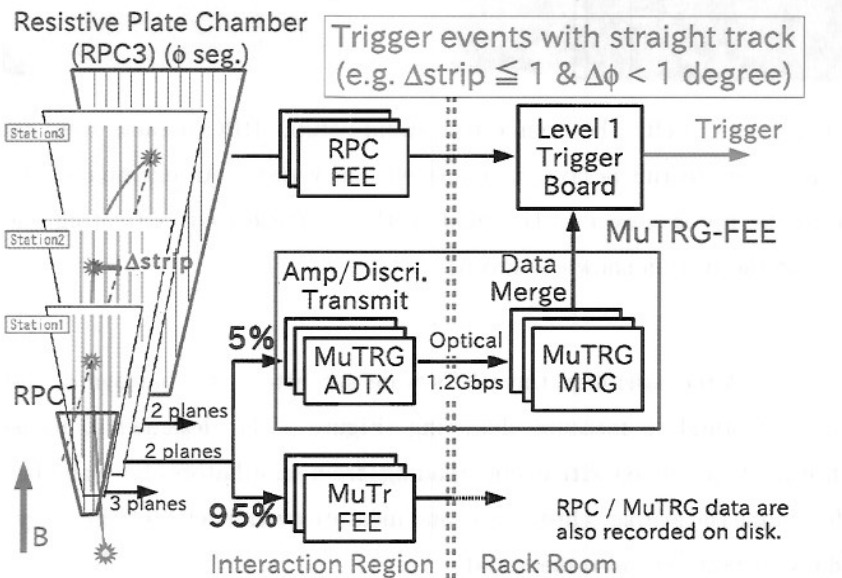


Figure 4.32: A schematic of the new muon trigger for recording W-Bosons [64]

#### 4.5.3.1 2013 Data Set Triggers

In general, when two protons inelastically interact, we do not care about the particles that are produced because they simply tell us about physics which we already understand. To learn about new physics, or to test models, we must devise a way to preferentially record this 'interesting' data, since data recording bandwidth is limited. A decision must be made within the time scale of one beam crossing (nanoseconds) whether or

*This is what we do not understand! even from "min bias" events ...*

81  
how do we define  
"interesting data"

be precise

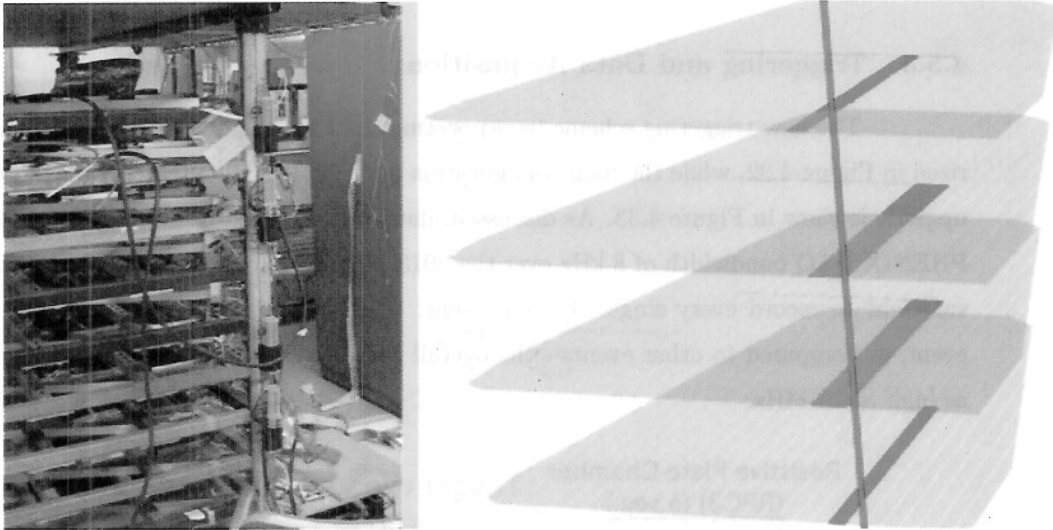
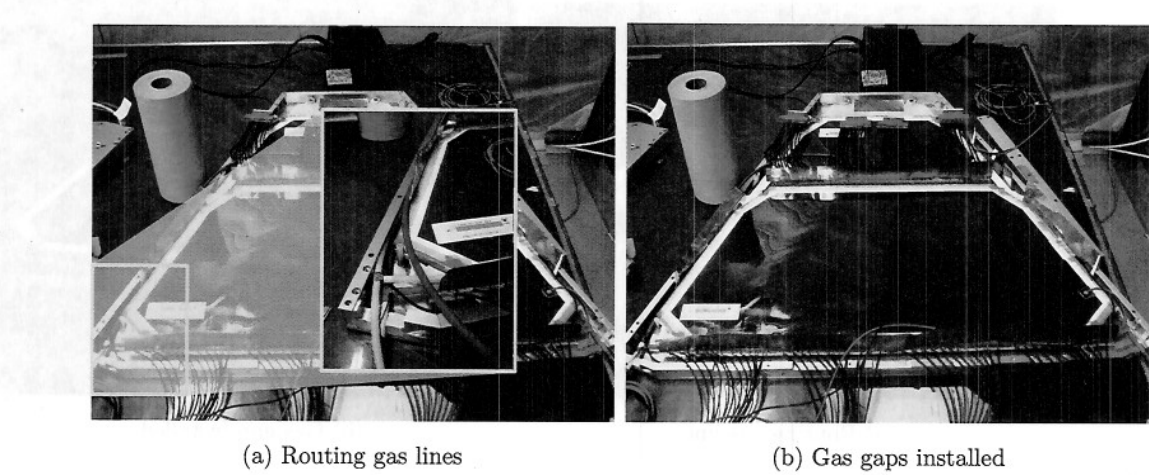


Figure 4.31: Left: the cosmic test stand setup. RPC octants were sandwiched between scintillators to run performance and efficiency tests. An example of the clustering due to a cosmic ray is shown on the right, with a particle (red) activating one or two strips per octant (activation shown in green).

After assembly, the RPCs were subjected to a barrage of tests, using a cosmic ray test stand to measure clustering (Figure 4.31), designed to measure the activation threshold (combined with energy readings from scintillators above and below the test stand), determine the average cluster size, and measure overall detector efficiency. The overall ohmic ‘dark-current’ was also measured.

#### 4.5.2.3 Performance

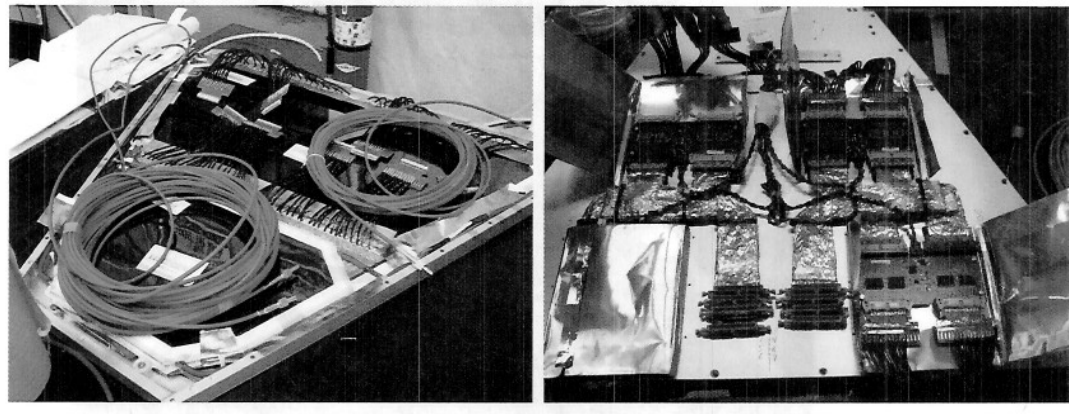
With the construction and installation of the RPCs and new Front End Electronics for the Muon Tracker, PHENIX was ready to take data for the W measurement by 2013. A dedicated run was taken, accumulating over  $200 pb^{-1}$  of data. All tolerances and design specifications for the upgrade were met.



(a) Routing gas lines

(b) Gas gaps installed

Figure 4.29: The final Bakelite gas gaps are installed on top of the copper readout strips. Gas lines are routed similarly to 4.27

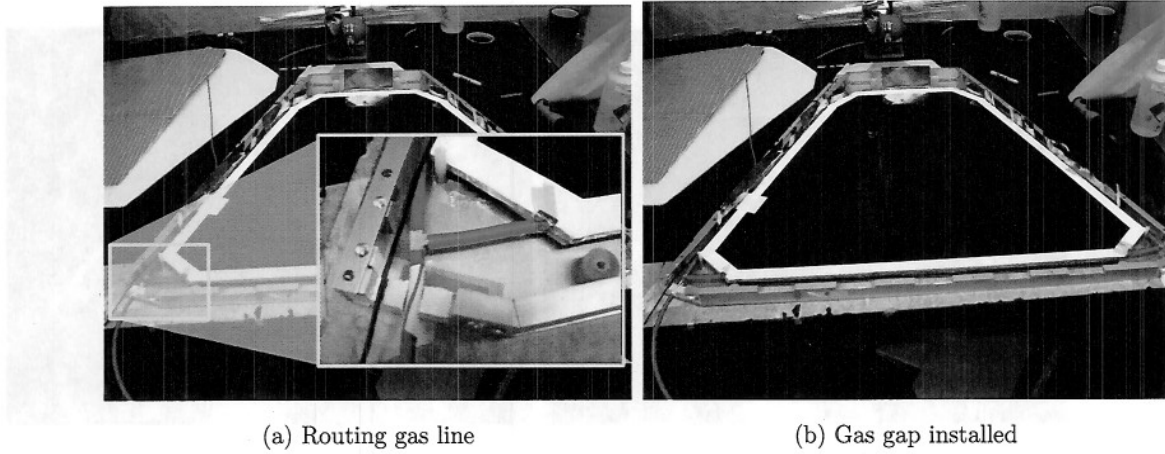


(a) Inside Assembly Complete

(b) Front-End Electronics Installed

Figure 4.30: A completed RPC 1 octant, interior assembly complete, left, and the outer assembly completed on the right.

# DRAFT



(a) Routing gas line

(b) Gas gap installed

Figure 4.27: The egress port of the gas gap is carefully shielded with tape to prevent friction from causing tears, and routed out of the ports machined into the bottom of the chassis (right), with the final position of the first gap shown on the left.

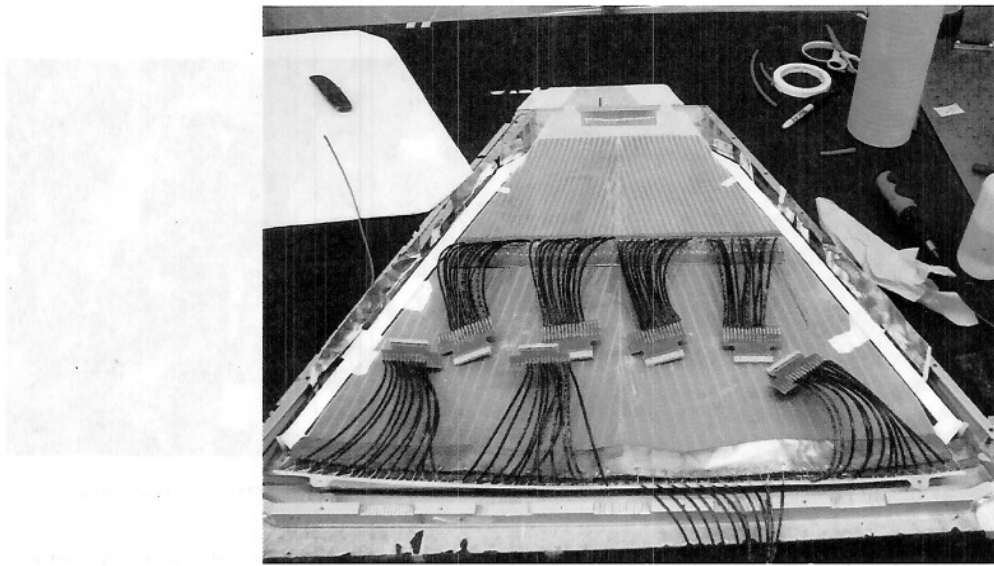


Figure 4.28: The copper readout strips are mounted to the chassis. Each readout strip is soldered to a copper wire, which in turn are gathered into readout chips.

# DRAFT

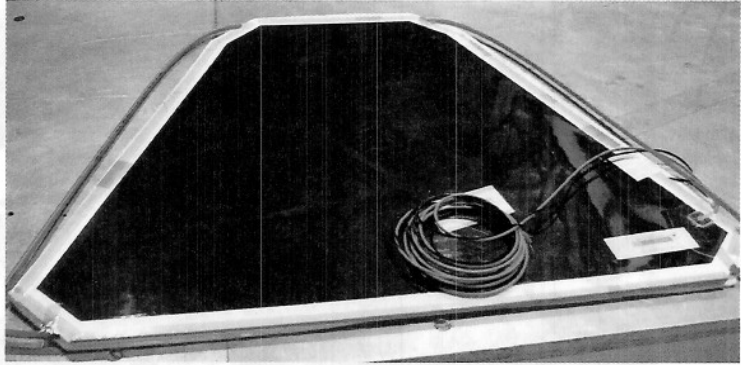


Figure 4.26: The assembled Bakelite gas gap, ready for leak/pop testing, followed by burn in.

the copper foil, such that they can be folded around the inner gaps, but not around the gas lines. The bias cables and gas lines are routed through the chassis side channels.

Once the bottom gas gap has been installed and secured, the copper readout strips are added, Figure 4.28. The strips are oriented such that two annuli of readout strips are created (azimuthally) when the RPC 1 is installed onto the nose cone of the muon trackers. The readout strips are designed this way as to offer some rough radial tracking. The copper readout strips are laminated with mylar, and each is soldered to its own channel, which are gathered and soldered onto PCB chips. The readout strips are laminated such that mounting holes in the laminate attach in the same way to each octant, for consistency.

Following the installation of the readout strips, the final two gas gaps are installed, with their electronics and gas lines routed through the chassis similarly to the bottom gap, Figure 4.29.

Finally, the high voltage cables are grounded to the chassis and soldered to the relevant wires leading to the graphite electrodes on the outside of the Bakelite gas gaps. Wires, tubes, etc. are all fixed in place with Kaptan tape. The top of the chassis is screwed into place, and the front-end electronics are installed, with the copper readout chips plugging into the relevant FEM board. Ribbon cables are appropriately routed, and all electronics are encased in copper foil, and then additionally protected with aluminum shells, Figure 4.30.

# DRAFT

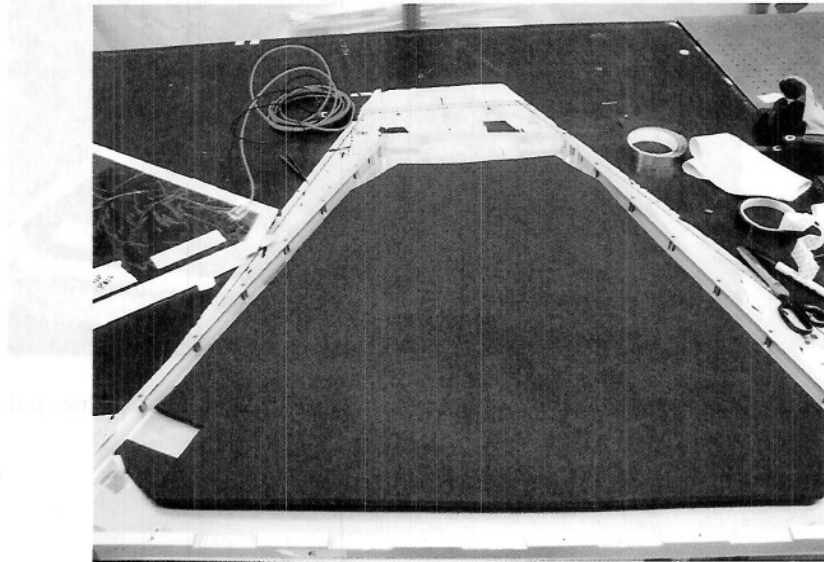


Figure 4.25: Foam shock insulation is added to the RPC 1 chassis.

separated by small insulating spacers. On the outside, the Bakelite is coated with graphite suspended in linseed oil to produce outer surfaces that can be held at a fixed voltage bias. The separation of the plates forms a chamber, which is sealed from the outside. Electrodes are attached to the linseed oil to allow for bias, and plastic nipples are routed into the gap chamber allowing for gas flow. Tubes are cut to size and fixed to the gas chamber nipples, and then routed out down to the widest end. These gas feed tubes are color coded - a different color for each Bakelite section in the RPC. These gas gaps are leak/pop tested in the lab. This test involved pressurizing the gaps to 8.5 inches of water, and measuring pressure loss over a ten minute interval, using Argon. Pressure losses less than 1 inch was acceptable. During pressurization, I checked for an audible pop sound, which indicated one of the gap spacers popping lose. Popping noises, or bad pressure retention would both result in the gas gap being discarded. Finally, before installing the gap, the gap was 'burnt in', a process where the gaps were filled with the physics gas mixture' and then slowly voltage cycled to operating voltage over 24 hours.

After the bakelite gas gaps are tested and have passed, they are installed into the chassis, Figure 4.27. The chassis is prepared for installation with the addition of a layer of copper foil, to create a Faraday cage around the sensitive bakelite gaps. Tabs are left on

# DRAFT

absolutely not  
affordable

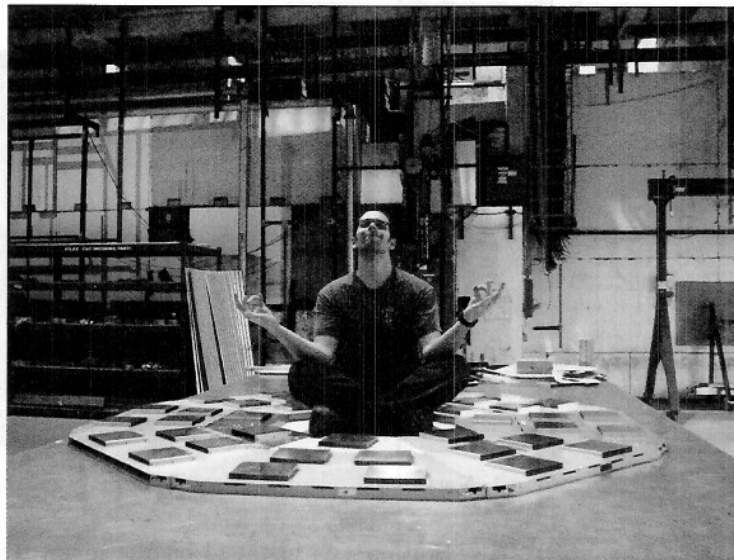


Figure 4.23: Here, we see one of the many hard-working physicists who tirelessly worked in building 911: a dusty, and irradiated construct built along the AGS beam-line. The physicist sits in the center of the RPC1 North chassis, for scale. More information can be found in [65].

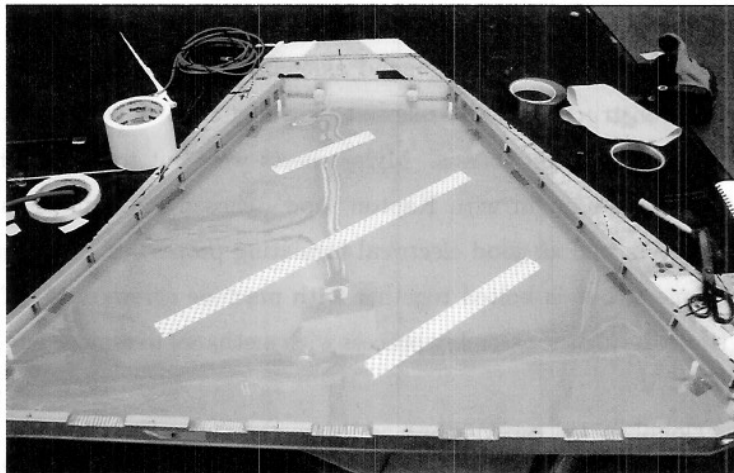


Figure 4.24: The chassis is prepared with insulating Kapton tape and mylar sheeting. The grooves along the bottom of the chassis are for routing cabling from the readout strips (shown later). The channels along the side of the chassis is for routing gas flow lines.

I don't think all these pictures are necessary.  
75  
maybe they should be in an appendix

# DRAFT

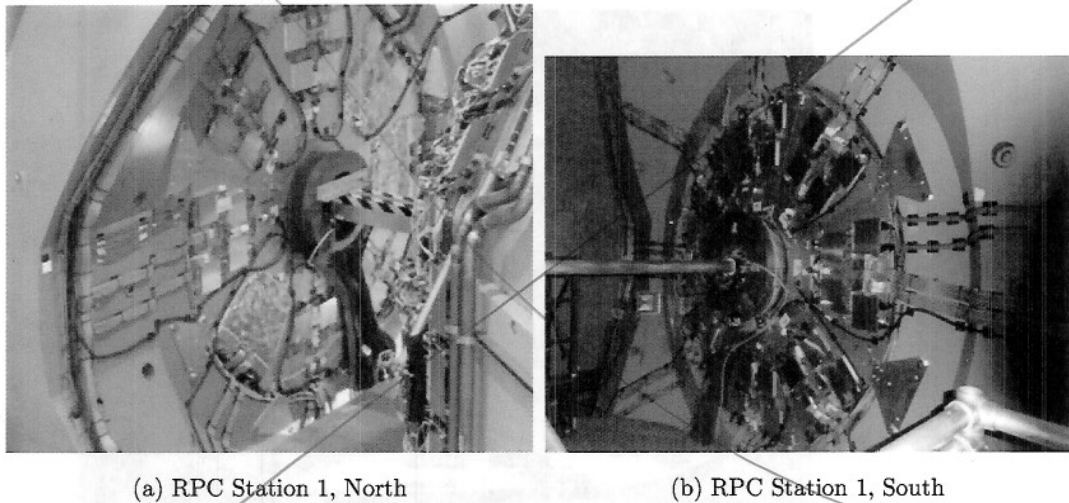


Figure 4.22: The North RPC Station 1 is installed on the muon tracker nosecone (left). Similarly we see the installation of the south RPC Station 1 (right). The metal tube in the center is the beryllium beam pipe.

and are the exact same size 4.23.

Each RPC1 octant was hand assembled, with components being tested at each stage of the construction, where relevant. The first stage of construction involved preparing the machined aluminum chassis. Mylar sheets were cut to fit the chassis baseplate, and secured to the aluminum with Kapton tape - chosen for robustness over high ranges of temperature, as well as good electrical insulating properties. The chassis itself is not one machined piece, but is bolted together with machine screws 4.24. The chassis is cleaned several times during the assembly process with methanol to remove any remaining machining debris.

Double-sided tape is then added to the mylar sheeting, and special foam is then placed down. Sections are removed from the foam to accommodate routing of the electrical hookup for setting the Bakelite gas gaps to a high bias, Figure ??.

After the chassis has been prepared, the bakelite gas gaps are assembled. The gas gap itself (Figure 4.26, Figure 4.20), is composed of two layers of Bakelite, which are

# DRAFT

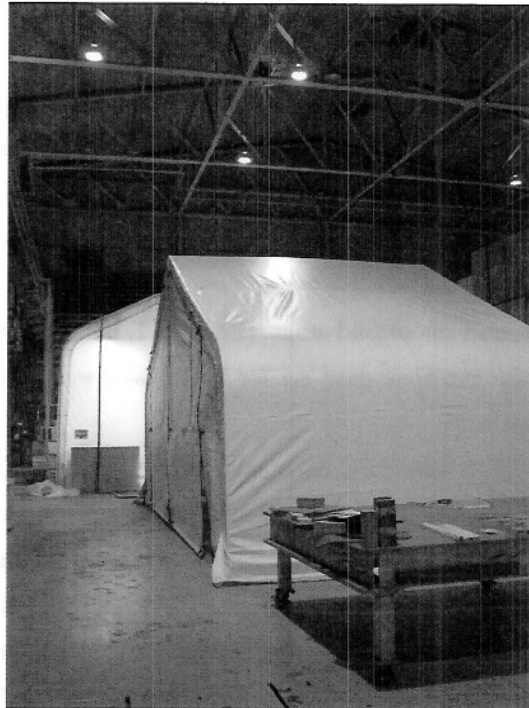


Figure 4.21: Two special tents inside building 912 at Brookhaven National Laboratory, built to house completed RPC octants and the laboratory used to construct and test the octants.

# DRAFT

Cluster Size	<2 strips
Efficiency	>95% for MIP
Time Resolution	~2 nanoseconds
Rate Capability	0.5 kHz/cm <sup>2</sup>

Table 4.3: The design characteristics of the RPCs [64]

### 4.5.2.2 Construction and Testing

Construction of the Resistive Plate Chambers took place in two stages over several years. Fabrication of the bakelite gas gaps was done overseas in Korea, and the aluminum chassis was manufactured in China. Pieces for the RPC 3 and RPC 1 were shipped to Brookhaven National Laboratory where they were assembled and tested, before being installed. The installation occurred over two years, with the first stage, the RPC 3, being installed in 2011, and the second stage, the RPC 1, being installed in 2012. After being fully commissioned, the capstone data set for W-Physics was taken in 2013, which is discussed in detail in Chapter 5.

The RPC 3 and RPC 1 construction efforts took place in a special clean-room built inside of the cavernous building 9-12 (Figure 4.21) at Brookhaven National Lab. Construction was overseen by Dr. Francesca Giordano, working as a post doctoral associate for Dr. Matthias Grosse Perdekamp for the University of Illinois at Urbana-Champaign. The electronics of the RPCs were funded by professors Ken Barish and Rich Seto at the University of California, Riverside, via a grant from the Department of Energy. I am very grateful for Francesca for her guidance and trust, as she allowed me to construct and test many of these octants. I constructed the gaps with Arbin Timilsina, who was a very entertaining and helpful lab-mate. Ihnjei Choi and Young Jin Kim were instrumental in the design, construction, and QA of the RPCs as well.

*actually?  
Young Jin?*

*what does this  
add? if you  
wish more to  
acknowledge your  
efforts*

The RPCs are modular in design - the larger RPC 3 North and South were separated into 16 half octants, whereas the smaller RPC 1 North and South were separated into eight octants. Both North and South RPCs have the same full azimuthal coverage, but due to the differing size of the Muon Arms, they have different rapidity coverage.

The RPC 1 octants were installed directly on the nose-cone of the Muon Tracker, shown in Figure 4.22. Unlike to the RPC 3, the RPC 1 North and South are quite compact,

→ You can have "different size" <sup>72</sup> AND some rapidity.  
you have to be much more precise with your statements...  
say what the intent is.

# DRAFT

-- (is 2^- not 1) everywhere!

## 4.5.2.1 Design

As hinted at prior, the design goal of the Resistive Plate Chambers is to provide accurate timing information at high speed in order to build a Trigger which can record  $W \rightarrow \mu$  events. RPCs were first implemented at the Large Hadron Collider at CERN, and their design has been adopted for use at PHENIX both because of its high speed, and low cost. In Figure 4.20 the basic design is shown. The means of signal transduction is via ionizing of gas inside a highly resistive chamber. The chamber is held at a large bias - at 8.5 kilovolts, such that any ionization will collect on the interior of the resistive chamber in a fixed, and relatively static distribution in time (relative to time scales of triggering system timing, in millionths of a second). This charge distribution is read out by capacitively coupled copper readout strips, into fast electronics (Figure 4.19). The design requirements of PHENIX is that when triggered, 2 or fewer clusters (strips) are activated, the efficiency of the detector must be at least 95%, the time resolution must be at least 2 nanoseconds, with a particle transduction rate of 500 Hz per square centimeter. These properties are summarized in Table 4.3 [64].

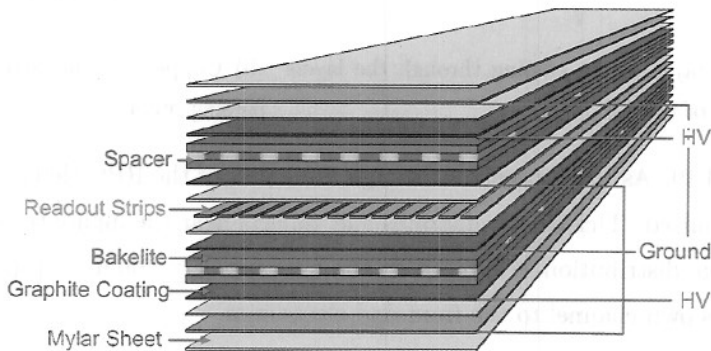


Figure 4.20: We can see the various layers that go into the construction of a typical RPC segment installed at PHENIX. A High Voltage bias is applied to the graphite coating on either side of bakelite gas-filled gaps. Readout strips are positioned between the two bakelite gaps. Finally, the entire double-gap structure is surrounded by a copper grounding cage, and wrapped in insulating mylar [64].

# DRAFT

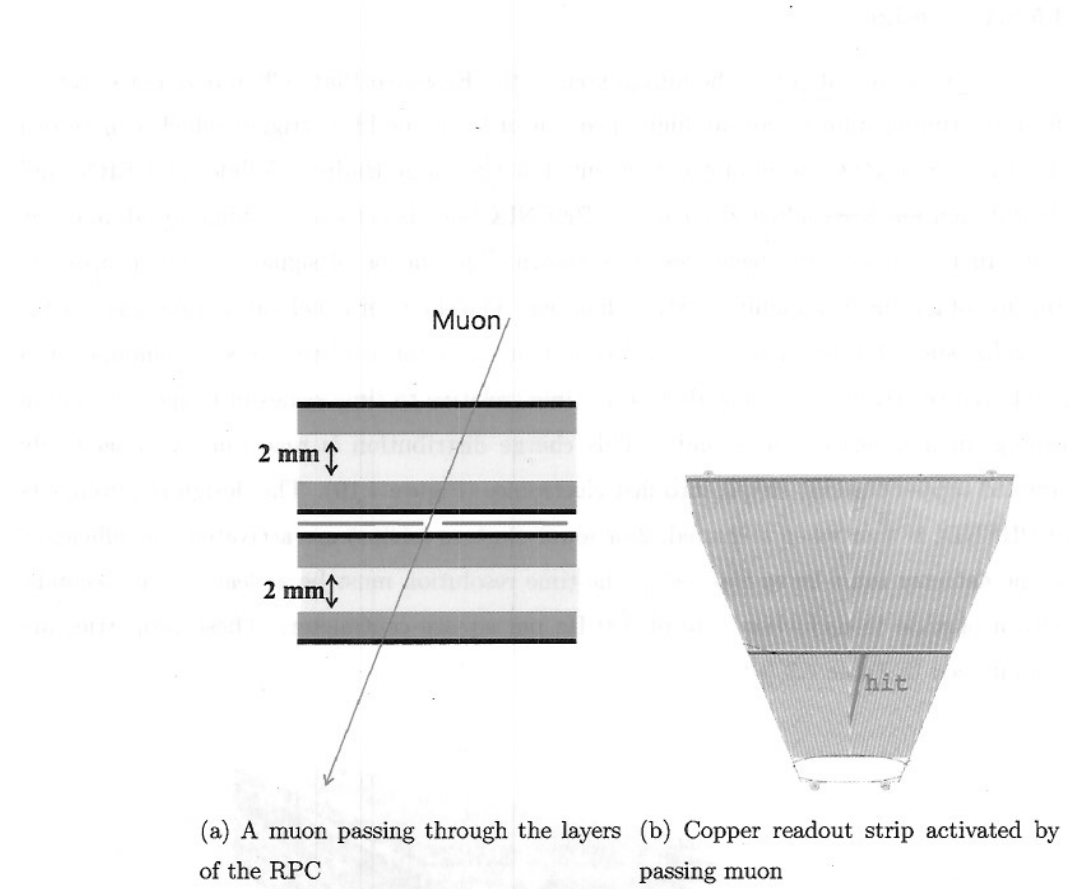


Figure 4.19: As a muon passes through the layers of the RPC (left), the gas in the bakelite gap is ionized. This charge migrates and collects near the highly resistive graphite coating. An image distribution is induced on the overlapping readout strip (right), which is passed along its own channel to the front-end electronics.

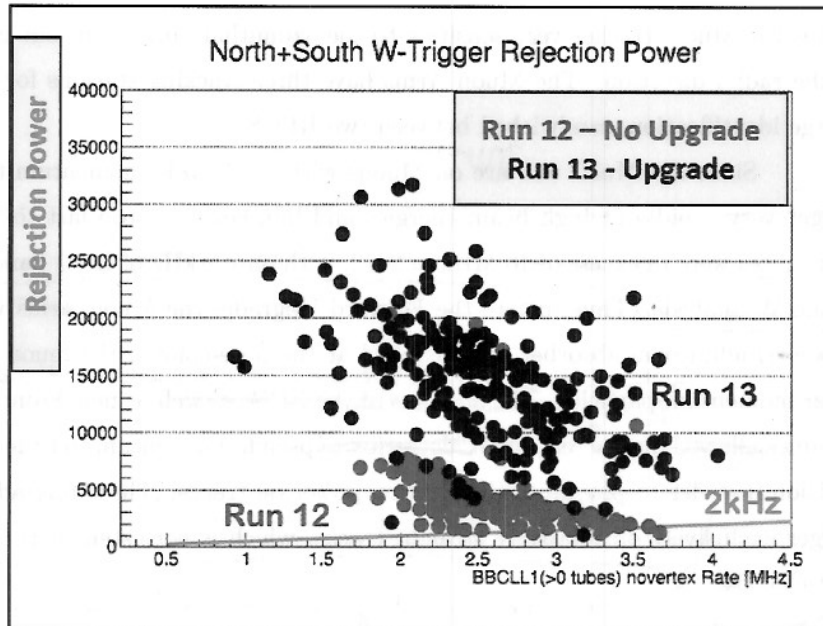


Figure 4.18: In 2013 with the final commissioning of the RPCs and the Forward Upgrade complete, we saw a ~~drastic~~ increase in rejection power, as planned.

*as expected.*

#### 4.5.2 The Resistive Plate Chambers

One of my major contributions to the PHENIX experiment was in the construction and testing of the RPCs at station 1, in 2012. An exploded view of the RPC is shown in Figure 4.20. The RPCs were a crucial part of the W-Physics muon trigger. One primary feature the presence of RPCs add to the PHENIX triggering system is timing resolution - 2 nanoseconds (Table 4.3). This is crucial, because before the inclusion of RPCs, the only timing available was that of the BBCs. However - because the BBCs are minimally biased - they will fire nearly every time there is a collision - which at high luminosity is far greater than the assigned bandwidth to the W Physics trigger. The RPC provides local timing information, which allows the triggering system to record events which trigger the muon arm system, and not just the BBCs. This has the effect of significantly reducing backgrounds - by a factor of > 6000 [64], Figure 4.18.

*ToF?*

*what does  
this have to  
do with  
anything?*

*so why is this important...*

*⇒ The real reason → they are RPCs (when attached to track)*

*ensures that you are patching on to the right bucket, so you know  
the size calibration ... Residual charge in MTR (slow & readout) could indicate  
fake tracks...*

# DRAFT

*Move some  
where*

makes the Muon Tracker very sensitive to the azimuthal dimension, but coarsely sensitive to the radial direction. The Muon Arms have three tracking stations for momentum and charge identification, sandwiched between two RPCS.

Since the MuID will fire on Muons with a  $2.5 \text{ GeV}/c$  momentum threshold, it will trigger very rapidly at high beam energies and luminosities - too fast to record all data - event rates were in excess of 10 MHz in 2013, with only 2 kHz of DAQ bandwidth allocated to the W analysis. Thus, before the Forward Upgrade, the Muon Arms were insufficient.

However, additional absorber was installed at the nose-cone of the muon tracker to block *these* lower momentum particles. The addition of the RPCs as well as new Front End Electronics Modules allowed for the real-time calculation of pseudo-momentum to be fed into the trigger decision in order to provide high rejection power on tracks. These upgrades allowed us to trigger exclusively on relatively straight tracks, which is consistent with high momentum particles [64].

*replaced existing muon tracker electronics to allow*

a high rate will be recorded, but biased toward non-W events. With event rates in excess of 10 MHz ... with MDS rates at ... (check in log book) almost no W events would be recorded as an active prescale (deliberate skipping of events) would suppress many signals. Not only do non-W events cause a trigger but a large number of "punch-through" hadrons also cause fake M triggers. To combat these hadrons,

*Can we describe this better & more precisely  
is exactly how the trigger works, its kind of  
important!*

# DRAFT

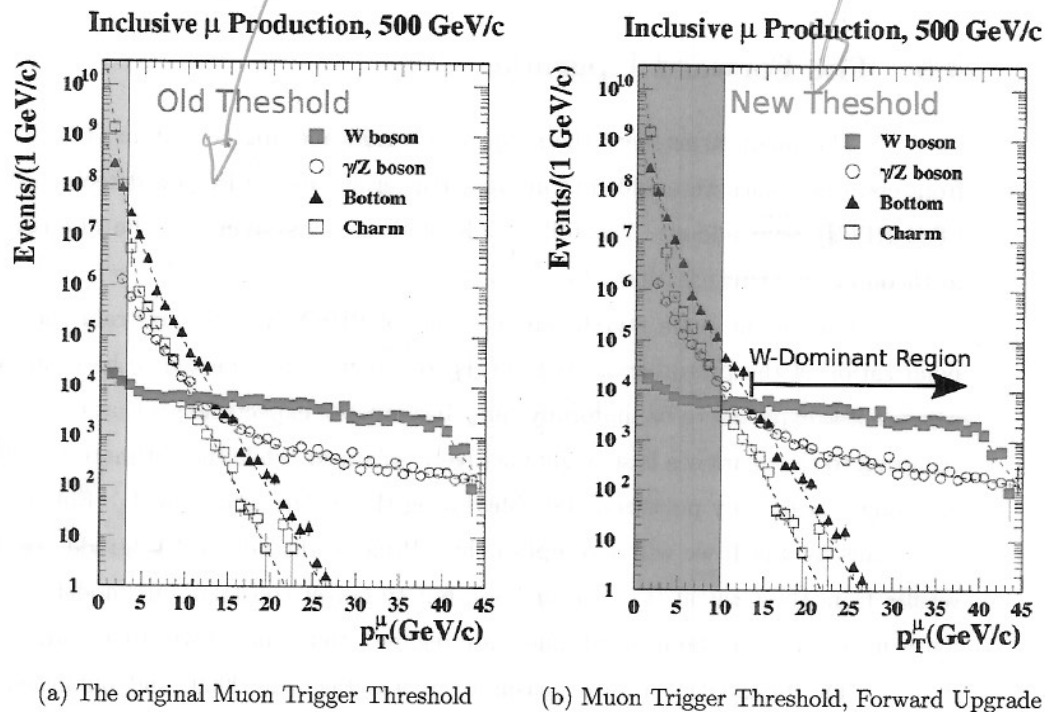


Figure 4.17: Observing the simulated production of muon as a function of  $p_T$ , we can see that in the kinematic region of  $W$  production that the dominant sources of muons come from other processes. The new PHENIX muon trigger threshold is sensitive at 10  $\text{GeV}/c$  and above. The threshold is still high enough that with other methods, we can record all events which come from the  $W$  boson, with triggering, whereas with the old threshold, this was impossible.

*it should be noted that ... background also accepted a type ...  
a substantial effort in this analysis, described in Section 6.4.*

**4.5.1 The Muon Tracker** Electronics (*Focus on "upgrade"*  
*the part*)

The primary purpose of the Muon Tracker is to reconstruct the energy and momentum of muons in the forward kinematic regime. Because the MuID is composed of larocci tubes sandwiched between solid steel sheets, only particles which penetrate all the layers of the MuID are identified as muons. The Muon Tracker has three cathode strip tracking planes in a volume of gas, with an applied radial magnetic field. Each plane has two faces of tracking strips, for six total tracking readouts total. The arrangement of cathode strips

*more  
Somewhere else  
(all of this  
not "upgrade")* *Are you talking about <sup>67</sup> muon tracker or muID?*

# DRAFT

This page needs a lot of work!

to where MuD?

## 4.5 The Forward Upgrade

The muon arms were the subject of significant upgrades from 2011-2013. New front end electronics were added to improve triggering, and entire new detector subsystems (The RPCs) ~~was~~ <sup>an</sup> ~~upgrades~~ <sup>new</sup> were added. The full details of these subsystems will be discussed in the ~~section~~ <sup>Why would you reference this current section?</sup> forthcoming sections (Section 4.5).

from the beginning  
of PHENIX?

One of the main stated physics goals of PHENIX is to constrain the sea-quark polarization of the proton spin. While this contribution is expected to be small, it is not because it is expected to be uniformly zero. Instead, the expectation is that the matter contribution to the quark sea is strongly positively polarized, while the antimatter contribution is strongly negatively polarized [48]. Measuring this polarization via  $A_L$  (Equation 3.5) is the means by which we will accomplish this. Prior to the Forward Upgrade, we only had results from the Central  $W \rightarrow \mu$  analysis, but to better constrain our models, we require lower uncertainty in the forward kinematic regime - thus, the Forward Upgrade.

The first data for this measurement was taken in 2009, and published in 2010 under [62] and [63], but only for central rapidities, where a clear Jacobean peak could be found in the electron invariant mass spectrum at  $40\text{ GeV}$  mass-energy (half the rest mass of the W-Boson). This made evaluating yields and calculating asymmetries relatively straight-forward.

However, in forward kinematic regimes, it was very difficult to discriminate real  $W \rightarrow \mu$  from other sources  $X \rightarrow \mu$ . As one can observe in Figure 4.17, only at high  $p_T$  does the W-boson signal become dominant. The old muon trigger electronics did not allow triggering sufficiently close to the W-Boson production threshold to allow for enough data to be taken. This is because of how the Muon Tracker identifies the charge and momentum of particles - which is via track bending. As tracks become very straight (i.e. high  $p_T$ ), the muon tracker struggles to reconstruct the correct charge and momentum. The original Forward Upgrade called for a nose-cone calorimeter, which would have helped greatly for particle rejection, but was canned for budget reasons.

The Forward Upgrade to PHENIX increased the muon triggering threshold from about  $2\text{ GeV}$  to  $10\text{ GeV}$ , enough to insure that all muons produced from W-Boson decays can be recorded, with no loss of statistics. This of course is not to say, that these events were recorded without any background processes - the removal of the muon background was

This is not quite accurate  
↓  
See help ↓  
Panel (a) shows the ~~at most~~ momentum spectra of several muonic decay processes, with the accepted trigger illustrating that the old electronics can allow mostly low momentum muons. Panel (b) shows the (then) expected threshold with new electronics.

# DRAFT

## 4.4.3.3 The Muon Arms

→ significantly expand - describe  
MuID & MSPEC (even more  
than next sect.)

which

The Muon Arms are composed of several subsystems, including the Muon Tracker (MuTR, cathode strip chambers), the Muon Identifier (MuID, shielding and scintillation layers), and the Resistive Plate Chambers (RPC(s), bakelite gas gaps and azimuthal oriented capacitively coupled copper readout strips). The job of the muon tracker is to identify muons with the penetration through the many layers of the MuID, and provide momentum and charge reconstruction for muon tracks. Tracks are matched to the event vertex with Kalman filter during reconstruction, and can even be matched with FVTX secondary vertices as a means of rejecting non W-Boson decays. Prior to the Forward Upgrade (Section 4.5), the muon arms consisted solely of the Muon Tracker and the MuID.

The Muon Tracker has a radial magnetic field, leading to charged particles traversing the tracker to have a helical bend. This was suitable for lower energy muon tracks, such as muons coming from the  $J/\Psi$  decay, which was one of the primary decays targeted in the original design of the muon tracker. detector from 3/4 to mu

However, these  $J/\Psi$  muons have much lower energy than muons which decay from ~~areal~~ W-Boson production. To extend the muon tracker's usefulness into tracking these high energy muons, an upgrade to the triggering system was required to obtain adequate back-ground rejection for the Forward W analysis. The details of the muon arms will be discussed in the next section.

*italic J, low energy +*

Do it here (next Sect. ii)  
"upgrade"

The muon tracker provides momentum and charge-sign reconstruction of charged particles impinging the detector. The MuID identifies photons by suppressing hadronic background (via absorption in the iron layers).

why do you need a trigger to reject background?  
why can't you do it off-line...

# DRAFT

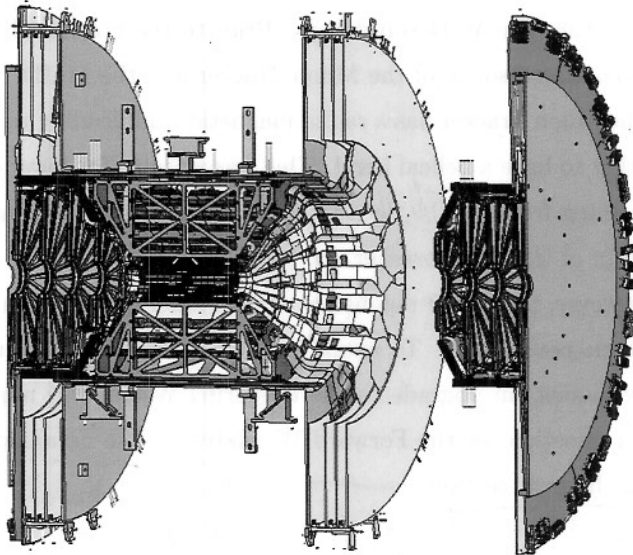


Figure 4.16: A schematic of the Forward Vertex Detector, showing the silicon chip layers (light blue wedges), and readout electronics (green). They are mounted directly onto the Silicon Vertex Detector, which was not used in this analysis. The FVTX and SVD together are used in heavy ion analyses [61].

*what do the "silicon chip layers" do compared to  
readout elec...*

*(more description or leave it out)*

# DRAFT

wrong way around

## 4.4.3.2 Forward Vertex Detector

(FVTX)

shown in

adds improves the

The Forward Vertex Detector, Figure 4.16 is a silicon detector, which provides additional tracking to detect secondary event vertices and additional precision to the Muon Tracking system. This detector can provide an important additional layer of precision, because it can help to identify events which do not originate from the primary event vertex of a collision, so they can be rejected from a pool of candidate  $W \rightarrow \mu$  events [61]. The properties of this detector are summarized in Table 4.2

Property	Value
Silicon sensor thickness ( $\mu\text{m}$ )	320
Strip pitch ( $\mu\text{m}$ )	75
Nominal operating sensor bias (V)	+70
Strips per column for small, large wedges	640, 1664
Inner radius of silicon (mm)	44.0
Strip columns per half-disk (2 per wedge)	48
Mean $z$ -position of four stations (mm)	201.1, 261.4, 321.7, 382.0
Silicon mean $z$ offsets from station center (mm)	5.845, 9.845

Table 4.2: A brief summary of the FVTX design parameters [61]

unless you explain what they mean  
or how they impact your analysis it  
just takes up space. I think something  
would be more appropriate, and easier than  
to Muon. Also reject factors would be  
useful, even if its from J/psi ...

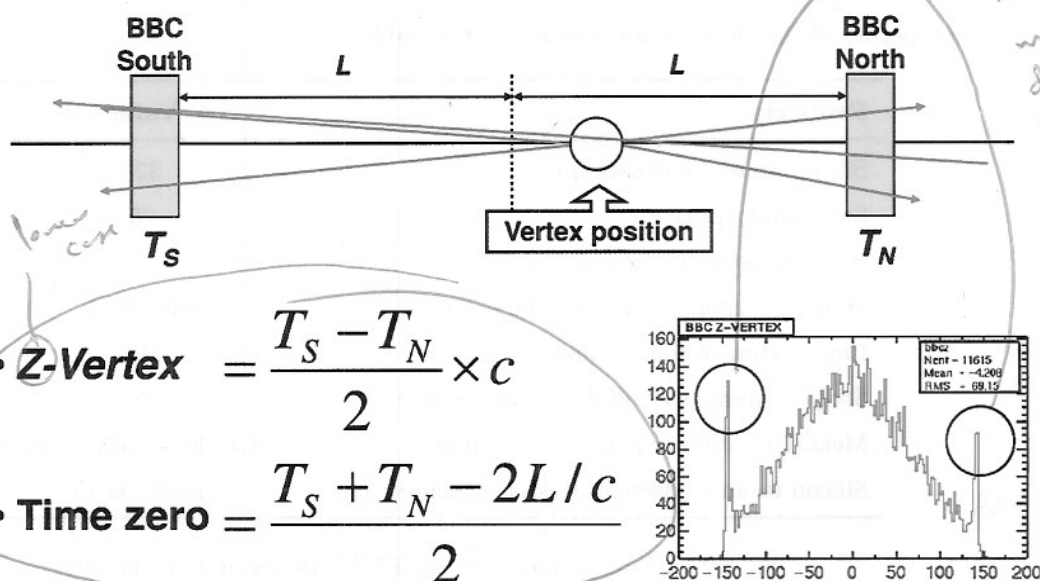
# DRAFT

All captions need to be in the form

"The top panel shows... Panel (b) illustrates..."

NOT

Pop: -- Left --



$T_{NS}$ : average hit time,  $c$ : light velocity,  $L$ : 144.35 cm

Figure 4.15: A diagram outlining the strategy for reconstructing the event z-vertex of a collision. Top: a cartoon of the North and South BBCs getting some particle penetration after an event. Bottom Right: a characteristic distribution of measured z-vertices for a short run taken in 2002 [60].

make a labeled formula  
line with the next  
then write it

Define this

# DRAFT

to journal  
 1 figure -  
 1 caption  
 (I had to resubmit  
 my thesis after  
 changing this)

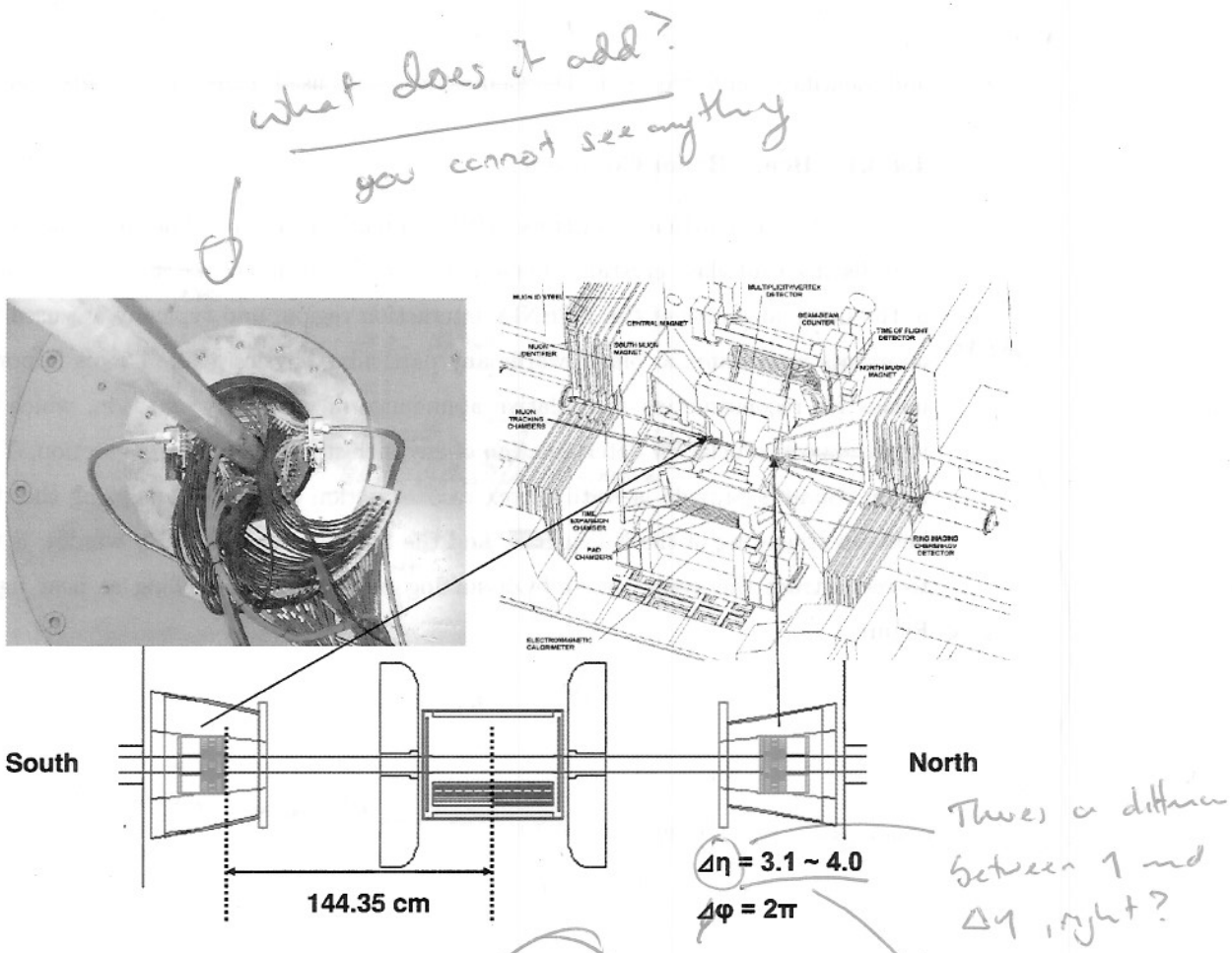


Figure 4.14: Shown: a photograph of the BBC hugging the beryllium beam pipe near the center of PHENIX (top left), a schematic showing the relative size and location of the BBCs as compared to the rest of PHENIX (top right), and a schematic of the exact proportions of the detector as viewed alongside the beam pipe (bottom), along with the rapidity and azimuthal coverage [60]

Photos The

there's a difference  
 (huge difference) between  
 rapidity & pseudorapidity

$3.1 \sim 4.0$   
 does not indicate precision

be precise...  
 $3.1 < \eta < 4.0$   
 (this side - check this)

I don't think you defined what  $\eta$  is did you

# DRAFT

I assume we have a precise definition?  
at some point?

For the complimentary central arm analysis, the  
and identification is required. The Central arms are used in the  $W \rightarrow e$  analysis. decay mode is  
explored.

## 4.4.3.1 Beam Beam Counters

The Beam-Beam counters (BBCs, Figure 4.14) are photomultiplier tubes with scintillating lead-glass crystals. These detectors are situated about 144 cm on either side of the nominal center of the PHENIX interaction region, and typically are used to trigger on events with minimal bias towards any particular physics goal. This is important as a means for reconstructing the relative abundance of particle production, which is as you might expect, crucial for determination of any inelastic scattering cross section. The Beam-Beam counters provide us with vertex reconstruction by way of analyzing the time delay between triggering of the North BBC and the South BBC. The delay window is then used to reconstruct the event vertex by assuming particles are travelling at near light speed, see Figure 4.15.

I changed as it sounds like the "events are minimal bias"

where  $T_0$  is  $\mu\text{Ts}$  is ...

# DRAFT

from page 55 → for final draft you  
need to fix such things...

can be found in Table 4.1.

## 4.4.2 The Spin Program

The PHENIX spin program was planned as part of the RHIC upgrade to produce polarized proton beams. The major analysis thrust of the PHENIX spin program has been to understand the spin structure of the proton, and has historically used various flavors of particle production asymmetries (left-right and forward-backward) as an experimental probe for polarized parton distribution functions (as we saw in Chapter 3).

Much of PHENIX collaboration's early published work focused on creating and studying quark gluon plasma in heavy ion collisions, but in following years spin papers came too. Major question in physics that PHENIX set out to answer with its heavy-ion program include studying confinement - i.e. why are quark color charges confined to exist in the nucleus, baryons and mesons? PHENIX sought to study this via examination of the  $J/\Psi$  and measuring screening length in heavy ion collisions. Additional research topics included the study of chiral symmetry restoration, thermal radiation of hot gasses, QCD Phase transition, Strangeness and Charm Production, Jet Quenching, and Space-time evolution [58].

The spin program came shortly after the 2001 commissioning run. The first polarized proton run was produced by RHIC for PHENIX in 2002, with 8.3 total weeks of data, run discontinuously. This was not as RHIC was still being optimized for spin physics... The primary goals of the PHENIX spin program are to study the polarization of the proton, specifically in the context of the Ellis-Jaffe sum rule, which decomposes the proton spin into various contributions from its substructure. The main structures studied by PHENIX are the gluon polarization,  $\Delta g$ , and the anti-quark polarization,  $\Delta \bar{q}$ . Additionally, the nature of parity non-conservation itself can be directly studied using polarized beams, and spin asymmetries in collisions. Though this measurement generally requires a means of reconstructing jets (PHENIX doesn't have this), inclusive or leading particle production can be used as a substitute with some small asymmetry remaining [59].

## 4.4.3 Subsystems

The major subsystems contributing to this work include the Muon Arms, the Beam Beam Counters (BBCs), and the Forward Vertex Detector, since the analysis is totally characterized with calculating the  $A_L$  for  $W \rightarrow \mu$  interactions, only muon reconstruction

Is it there  
- neutrino is here -

# DRAFT

*digested*

Element	$\Delta\eta$	$\Delta\phi$	Features
<b>Magnets</b>			
Central Magent	$\pm 0.35$	$360^\circ$	$1.15 T$
Muon Magnet North	$-1.1 - -2.2$	$360^\circ$	$0.72 T$
Muon Magnet South	$1.1 - 2.4$	$360^\circ$	$0.72 T$
<b>Minimum Bias</b>			
Beam Beam Counter	$\pm(3.1 - 3.9)$	$360^\circ$	Vertex Reconstruction
Zero Degree Calorimeter	$\pm 2mrad$	$360^\circ$	Minimum Bias Trigger
<b>Central Detectors</b>			
Drift Chambers	$\pm 0.35$	$90^\circ \times 2$	Central $p$ and $m$ resolution
Pad Chambers	$\pm 0.35$	$90^\circ \times 2$	Pattern Recognition, Tra
Ring Imaging Čerenkov	$\pm 0.35$	$90^\circ \times 2$	Electron ID
Time of Flight	$\pm 0.35$	$45^\circ$	Hadron ID, $\sigma < 100m$
PbSc EMCal	$\pm 0.35$	$90^\circ - 45^\circ$	Calorimetry, photon and elect
PbGl EMCal	$\pm 0.35$	$45^\circ$	$e^\pm, \mu^\pm$ separation at $p > 1GeV/c$ , EM Shower and $p < 1GeV/c$
<b>Muon Arms</b>			
Muon Tracker South	$-1.15$ to $-2.25$	$360^\circ$	North installed 2003
Muon Tracker North	$1.15$ to $2.44$	$360^\circ$	
Muon ID South	$-1.15$ to $-2.25$	$360^\circ$	Steel absorbers, larocci t
Muon ID North	$1.15$ to $2.44$	$360^\circ$	"

Table 4.1: A summary of PHENIX hardware [57]. Electron/pion separation and Pion/Kaon separation requires the Time of Flight (ToF) working with PbGl and PbSc data. PbGl refers to "Lead Glass Scintillator" and PbSc refers to "Lead Scintillator". The Muon Identifier (Muon ID, MuID) can help separate muons from hadrons.

actually it cannot  
it suppresses the hadrons by  
absorbing them in the iron

$e^\pm/\pi^0$  does not require ToF  
 $e^\pm/\pi^\pm$  does, but depends on mom.

# DRAFT

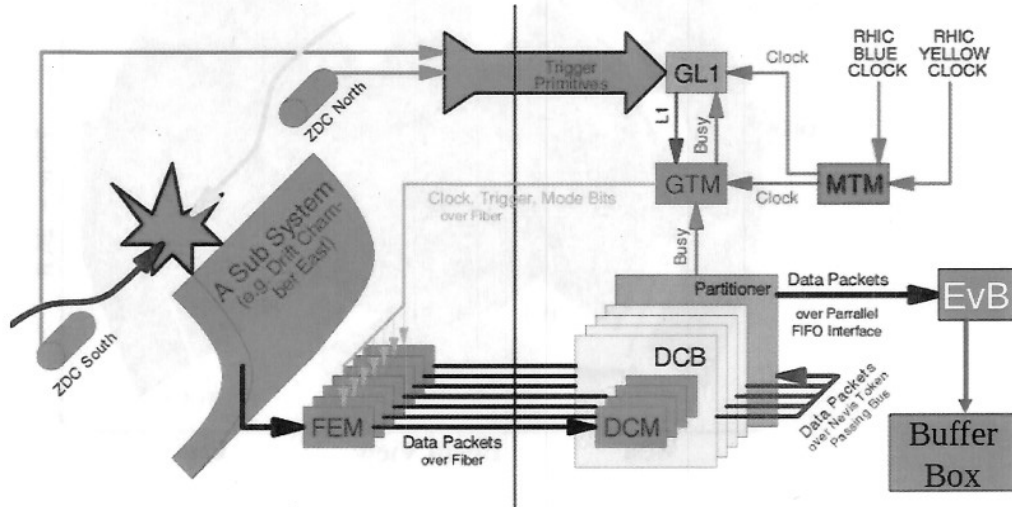


Figure 4.13: A flow chart summarizing the PHENIX DAQ [56]. From left to right, we can get a feel for the data flow at PHENIX. Shown is an event, the red splat on the far left. Particles from this event are transduced by a detector ('A Sub System'). The transduced signals are serialized into a detector specific data stream, such that the state of the detector's excitation can be recorded and reproduced later. This information is stored on the front-end-electronics modules (FEMs), and synchronized with timing information from the clock (ticks once every time there is a bunch crossing) and a Global Trigger decision, i.e. whether or not the right parts of the detector <sup>are triggered</sup> ~~are triggered~~ to make this particular event worthy of keeping. After this, if the event is deigned by the heuristics to be worthy of keeping, the uncompressed serialized information is sent to the DCMs, where it is assembled into a packet, and then sent to the event builder (EvB), where all packets sharing a common collision are assembled into an event. The event is compressed into a proprietary (PRDF) format, and sent to the Buffer Boxes, which are a cache of high density local storage, which is later sent off to cold storage on magnetic tape drives.

# DRAFT

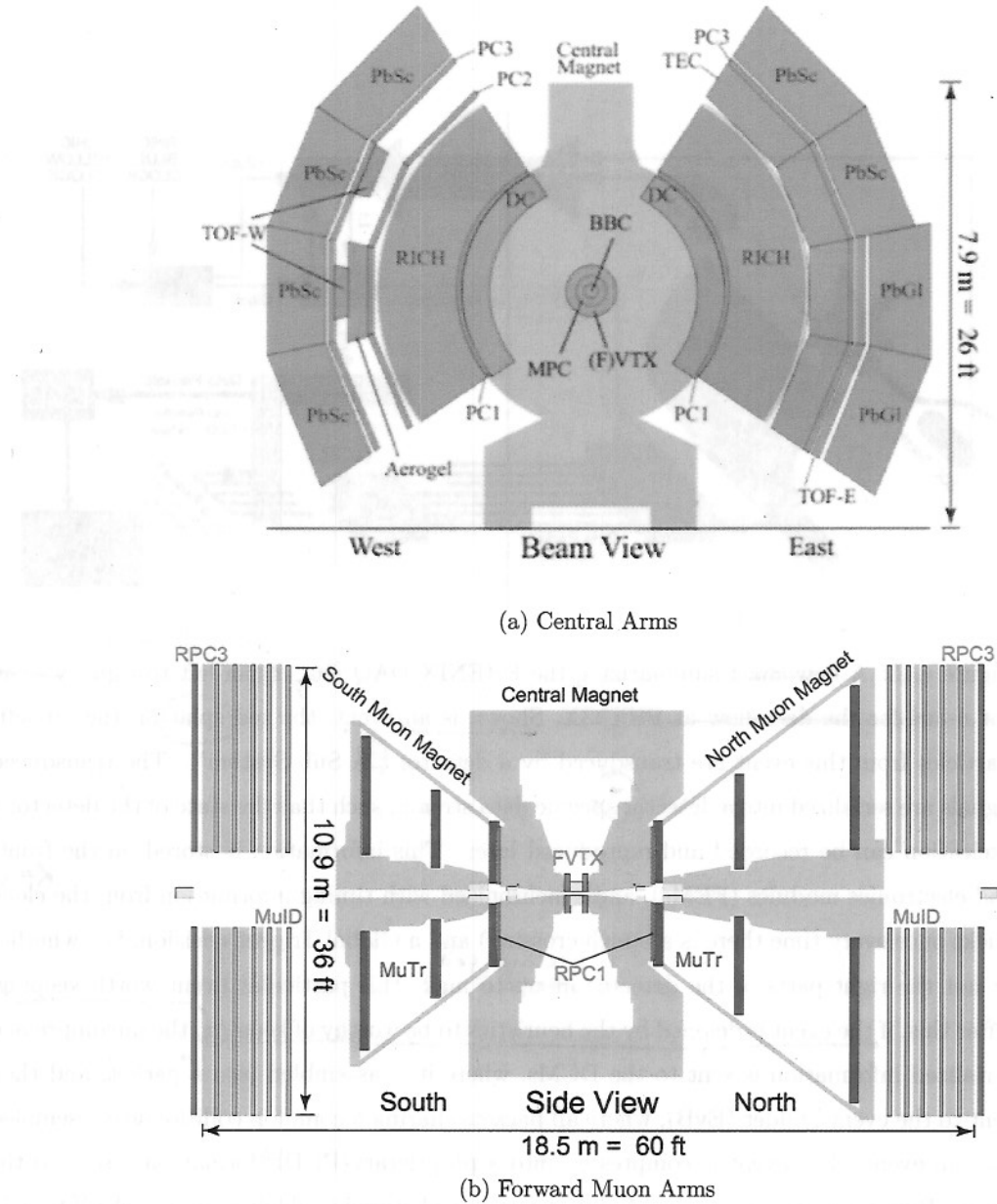


Figure 4.12: Shown: The two main halves of the PHENIX Spectrometer. The central arms are shown via the beam-on view of PHENIX (left) and Forward Muon Arms are shown via the 90-degree rotated view. In both cases, the 2013 configuration is shown. The beams are brought into intersection at the geometric center of each figure (immediately between the BBCs)

# DRAFT

## 4.4 The Pioneering High Energy Nuclear Interaction Experiment

### 4.4.1 Overview

The Pioneering High Energy Nuclear Interaction Experiment is a synthesis of many smaller detectors all of whom were commissioned for various physics goals; some of which have been repurposed from their original application once the primary physics mission of the detectors were completed.

The configuration of the PHENIX spectrometer can be changed from year to year, depending on the analysis needs of the physics working groups. The configuration of the detector for the 2013 physics run is shown in Figure 4.12.

PHENIX makes use of many classic detector technologies, it contains Čerenkov light detectors, resistive plate chambers, electromagnetic calorimeters, silicon chip detectors, time of flight detectors, scintillation light detectors, cathode strip chambers, and proportional tube counters.

While all of these subsystems are interesting, and have produced excellent physics results, I will focus only on those pertinent to this analysis.

PHENIX is generally thought of as two 'halves', which often are used in separate analyses - the forward muon arms, and the central arms. While both halves are used for both heavy ion, and spin physics analyses, this analysis exclusively uses the forward muon arms, so the central arms will not be discussed (though, a closely related analysis, dealing with  $A_L$  for  $W \rightarrow e$  exclusively uses the central arms). The different subsystems cover different rapidity ranges, so many times, complimentary results are obtained from central and forward analysis. Results from such a complementary central analysis will be presented alongside my results in later chapters.

PHENIX also utilizes a complex data acquisition system (DAQ) which streams data from each detector, assembles this data into a labeled event, compresses, and stores into a proprietary storage format. The work-flow of this is summarized in Figure 4.13. A complete summary of PHENIX detector subsystems (excluding the Forward Vertex Detector, Silicon Vertex Detector, and Resistive Plate Chambers, which are new, and discussed separately)

# DRAFT

spin-quality of the live data, Figure 4.11



Figure 4.11 shows the distribution of spin-quality values for the live data. The distribution is roughly symmetric and centered around a spin-quality of 0.55. This indicates that the live data is generally of good quality, with most events having a spin-quality between 0.4 and 0.7.

The distribution of spin-quality values for the live data is shown in Figure 4.11. The distribution is roughly symmetric and centered around a spin-quality of 0.55. This indicates that the live data is generally of good quality, with most events having a spin-quality between 0.4 and 0.7. The distribution of spin-quality values for the live data is shown in Figure 4.11. The distribution is roughly symmetric and centered around a spin-quality of 0.55. This indicates that the live data is generally of good quality, with most events having a spin-quality between 0.4 and 0.7.

The distribution of spin-quality values for the live data is shown in Figure 4.11. The distribution is roughly symmetric and centered around a spin-quality of 0.55. This indicates that the live data is generally of good quality, with most events having a spin-quality between 0.4 and 0.7.

The distribution of spin-quality values for the live data is shown in Figure 4.11. The distribution is roughly symmetric and centered around a spin-quality of 0.55. This indicates that the live data is generally of good quality, with most events having a spin-quality between 0.4 and 0.7.

The distribution of spin-quality values for the live data is shown in Figure 4.11. The distribution is roughly symmetric and centered around a spin-quality of 0.55. This indicates that the live data is generally of good quality, with most events having a spin-quality between 0.4 and 0.7.

The distribution of spin-quality values for the live data is shown in Figure 4.11. The distribution is roughly symmetric and centered around a spin-quality of 0.55. This indicates that the live data is generally of good quality, with most events having a spin-quality between 0.4 and 0.7.

The distribution of spin-quality values for the live data is shown in Figure 4.11. The distribution is roughly symmetric and centered around a spin-quality of 0.55. This indicates that the live data is generally of good quality, with most events having a spin-quality between 0.4 and 0.7.

The distribution of spin-quality values for the live data is shown in Figure 4.11. The distribution is roughly symmetric and centered around a spin-quality of 0.55. This indicates that the live data is generally of good quality, with most events having a spin-quality between 0.4 and 0.7.

The distribution of spin-quality values for the live data is shown in Figure 4.11. The distribution is roughly symmetric and centered around a spin-quality of 0.55. This indicates that the live data is generally of good quality, with most events having a spin-quality between 0.4 and 0.7.

# DRAFT

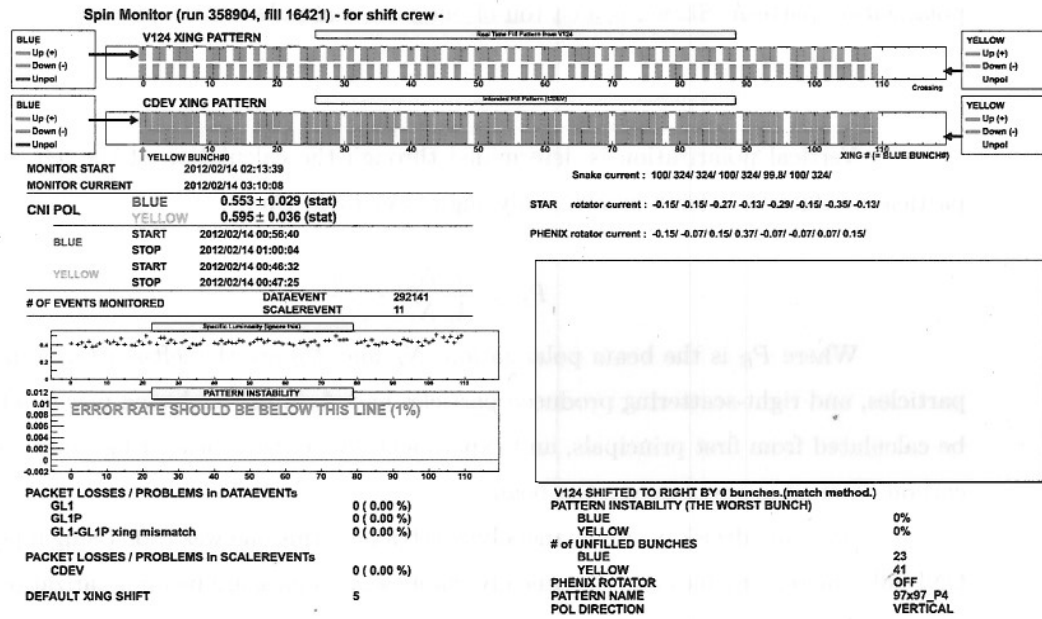


Figure 4.11: The shift-crew display output for the Spin Monitor. The upper panel shows the polarization of the blue and yellow beams, and other panels summarize information including magnet currents (needed to understand the spin orientation), issues with data packet loss, the recognized spin-pattern, as well as a large boxed area on the lower left where errors could be shown to the shift crew along with the proper response.

# DRAFT



Figure 4.10: As beams are longitudinally rotated into position for collision, it is crucial to keep careful track of the magnet currents rotating the beams, as well as the overall polarization pattern. Shown is a cartoon of one potential polarization pattern.

Vertical polarization is determined through the calculation of the left and right particle production, with a known analyzing power ([54], Ch 8):

$$P_B = \frac{1}{A_p} \frac{N_L - N_R}{N_L + N_R} \quad (4.1)$$

Where  $P_B$  is the beam polarization,  $N_L$  and  $N_R$  are the left-scattering produced particles, and right-scattering produced particles and  $A_p$  is the analyzing power, which can be calculated from first principals, and experimentally verified. Scattering takes place as a carbon filament is swept across the beam.

As many decisions are financially constrained, this one was too. Using a p-Carbon CNI polarimeter provides an economically viable way to measure beam polarization within the precision needed for the spin experiments.

### 4.3.2.1 The Spin Monitor

One of my major contributions to the PHENIX experiment was in the upkeep and development of the spin monitoring systems for the online data taking portions of the experiment. *see fig 4.11*

During a RHIC run, it is crucial to keep track of the polarization patterns being collided at the PHENIX IR 4.10

The spin monitor was composed of tens of thousands of lines of code, and was quite a monstrosity to keep running, however, I managed it. I contributed better error logging, and helped to facilitate a total rewrite of the software, to create more understandable and reliable output. However, in the interim, I reprogrammed the monitor to handle spin patterns, and provide the shift crew at PHENIX with immediate feedback regarding the

## 4.3 Maintaining Beam Polarization

The creation of polarized beams is only half the battle. Depolarizing resonances in any particle beam are intrinsic in the design of any circulating beam particle accelerator - without intervention, after a few rotations, RHIC's polarized beams would be unpolarized. RHIC uses several strategies in concert to correct for the largest of these depolarizing resonances - including beam orbit corrections, the Siberian Snakes, Betatron Tune Spreading, and sextupole magnetic depolarizing resonances.

### 4.3.1 Siberian Snakes and Spin Rotators

The Siberian Snakes are positioned at two locations on the RHIC ring (as well as others along the injection sequence). The most stable configuration of spin injected in RHIC is such that the spin axis is perpendicular to the plane of the accelerator ring. The Siberian snake is a helical magnet which forces the spin to rotate 180 degrees every half rotation. This special configuration of snakes (see Figure 4.1) ingeniously takes advantage of the rotational precision of the spin (a depolarizing resonance) to re-polarize the beam, every half-orbit.

The spin rotators are located outside of experimental interaction regions around PHENIX and STAR. These special dipole magnets rotate the spin of the beams onto a longitudinal (parallel with beam) axis - these magnets are important for any measurement (such as this one) requiring longitudinal spin polarization. Otherwise, transverse spin effects can be studied, *at second distinct beam passes at RHIC.*

### 4.3.2 Measuring Beam Polarization

The RHIC Collider-Accelerator Department provides several means of measuring the beam polarization over the course of the data taking period. PHENIX takes special data and studies it, to determine the real beam polarization delivered to the detector, *in a yearly analysis (for years where polarized data is taken).* This analysis is often called "Local Polarimetry", but is often abbreviated as LPol in PHENIX logs.

CAD will additionally measure polarization in via inelastic proton-carbon scattering in the Coulomb-Nuclear Interference (CNI) region. Relative polarization can be determined with to within 10% in only a few seconds of measurement.

# DRAFT

## 4.2 AGS-to-RHIC Transfer Line

The AGS-to-RHIC transfer line consists of two main sections: the AGS-to-Injector section and the Injector-to-RHIC section. The AGS-to-Injector section includes the AGS, a vertical bend, a horizontal bend, and a switching magnet. The Injector-to-RHIC section includes a vertical bend, a horizontal bend, and the RHIC. The total length of the transfer line is approximately 1.7 km.

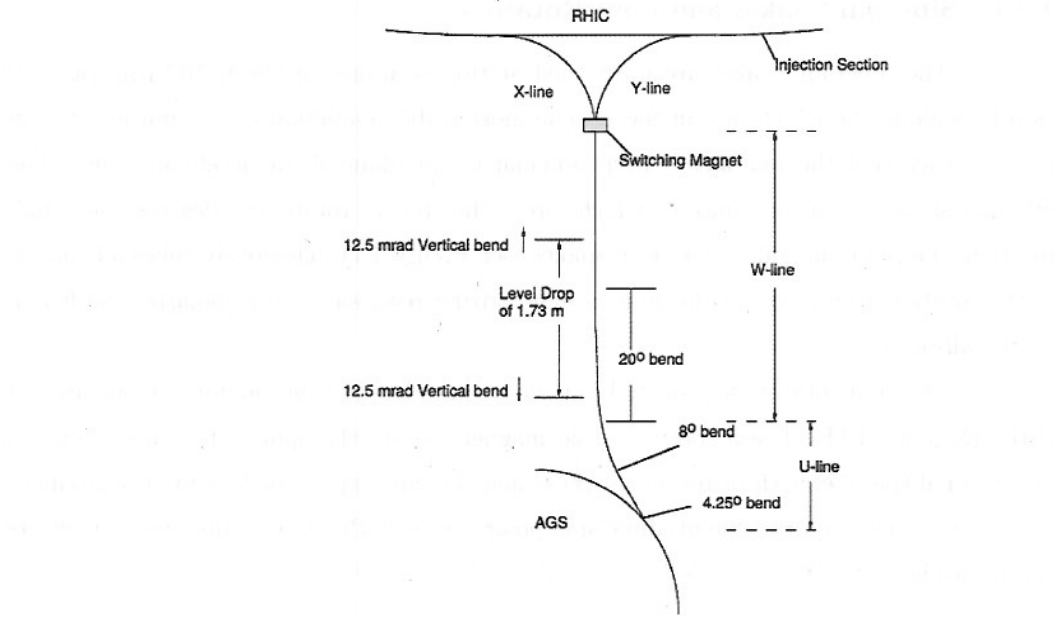
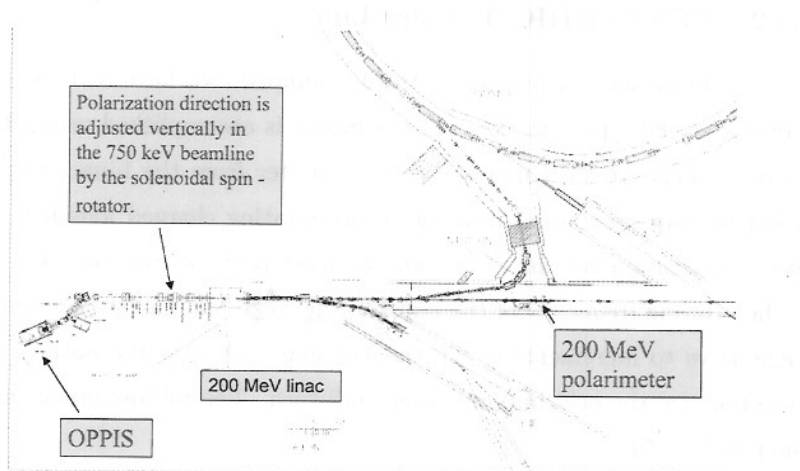
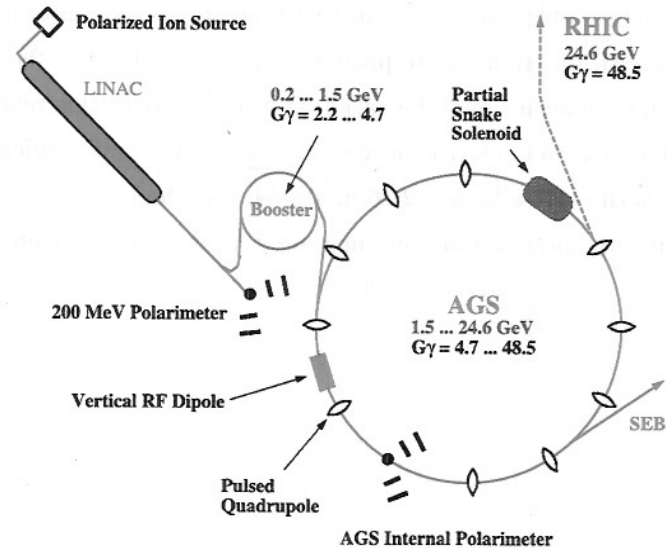


Figure 4.9: A schematic of the geometry of the AGS-to-RHIC transfer line [54].

# DRAFT



(a) Technical schematic of Polarized Injection Line [55]



(b) Overhead view of Polarized Injection Line [54]

Figure 4.8: A view of the RHIC polarized injection system. We see a zoomed in technical view of the OPPIS to the booster (a), below, we see a zoomed out cartoon of the next step in the polarization injection system, including the AGS, and the feeder line to RHIC.

# DRAFT

in RHIC not?  
ATR?

(Section 4.3)

## 4.2.2 AGS to RHIC Transfer Line

Once ions have been optically pumped, we have a direct-current beam at approximately 80% polarization. The pumping is accomplished using Rubidium vapor. The polarized ions are then moved into the booster from the Linac, where some polarization is lost to spin precession, intrinsic to accelerating charged ions in a circular path. However, polarization is maintained, for the most part, by matching the precession resonance to the orbiting frequency of the booster ring. The Siberian snakes and spin rotators at this stage serve to incrementally flip the ion spin such that the natural depolarization works to re-polarize the orbiting ions, every full-turn. The full details of this procedure are well described in [54].

After the ions are sufficiently polarized and filled in the AGS, they are moved into the AGS to RHIC Transfer line, Figure 4.9. The beam is focused and fed through a switching magnet - which must be timed with great precision in order to fill the blue and yellow beams with the appropriate polarization patterns. In fact, the precision is so great, that the earth's curvature must be taken into account over this relatively short injection line - the entry point and exit point are bent ever so slightly different - the entry being 12.51 mrad, vs the egress being 12.46 mrad [54]. At the point of injection in the transfer line, the beam size and emittance are measured, as well as the beam polarization.

Spell out

DRAFT

© 2009 The Authors. Journal compilation © 2009 Association for Child and Adolescent Mental Health.

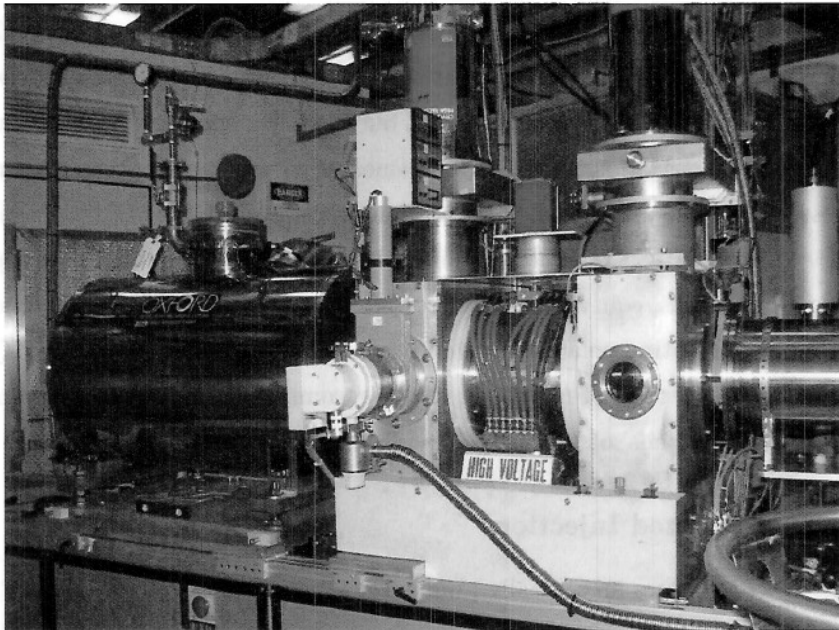


Figure 4.7: RHIC's optically pumped polarized ion source. Produces 0.5-1.0 mA current of polarized  $H^-$  ions. The optical pumping is pulsed at 400  $\mu$ s, [55]

# DRAFT

## 4.2 Production of Polarized Proton Beams

The production of polarized beams is crucial to the physics of this measurement without polarized beams, no spin structure analysis can be done at RHIC. This is due to the fact that the helicity state of the protons in the initial state of any proton proton collision can be connected to the final observed states in a way which provides information about the spin structure function, as was discussed in section 3.

The production of polarized beams is a multistage process, and involves several experimental components. The importance of polarizing the beams is fully realized once polarized beams are collided at relatively high center of mass energies - where the beams behave less like polarized proton beams, but more like polarized beams of quarks and gluons [53]. Beam polarization is achieved incrementally - with polarization starting as soon as the booster and AGS stage of the acceleration process 4.1. *Isn't it a polarized source?*

*Sentence doesn't make sense!*  
The RHIC Configuration Manual [54] provides a wealth of information, accelerator physics, diagrams, equations, and descriptions of the extremely precise and comprehensive approach to creating polarized proton beams and injecting them into RHIC. This work was crucial to this section of my thesis, and is recommended reading for anyone who wishes to know 'all the details' of how RHIC handles polarized beams.

*For more details see [54].*

### 4.2.1 Polarized Injection

RHIC uses an optically pumped polarized ion source (OPPIS), Figure 4.7 to produce a polarized ion source greatly in excess of RHIC's design intensity. This is used to our advantage, as the emittance of the beam can be lowered to create a highly collimated beam for physics use.

# DRAFT

With many millions of particles in each bunch, detailed beam dynamics studies are used to predict the beam properties to ensure the RHIC collision parameters are met.

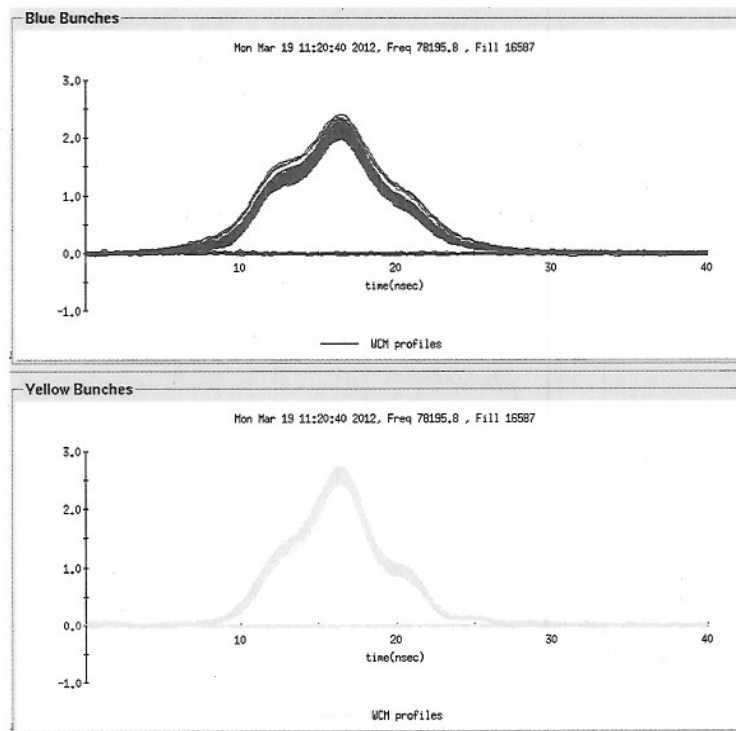


Figure 4.6: Plot courtesy of Angelika Drees, of RHIC's Collider-Accelerator department. The blue beam (blue) and yellow beam (yellow) are overlaid over a 40 nanosecond time period. Even with bunches crossing a fixed point over 40 nanoseconds, this still corresponds to an overall bunch length of about 12 meters. Conversely, the bunch width is quite narrow with Gaussian geometry, it is between 150 millimeters and 300 millimeters depending on the beam energy. Understanding the beam bunch geometry is a crucial component to understanding total the total luminosity delivered by RHIC to PHENIX.

*you should not  
name people... in  
ref. or acknowledgments...*

# DRAFT

'bunch' - and are rather long - Figure 4.6. A detailed presentation of beam dynamics with regards to luminosity will be presented in chapter 8.



speed range. The current is labelled as  $\text{mA}$  (milliampere) and the beam length  $\text{mm}$  (millimetre). The beam length is decreasing, the current is increasing, which corresponds to more and more charged particles in the bunch. In the beginning, the current is low and the beam length is large. This corresponds to a low current density. As the current increases, the beam length decreases, which corresponds to a higher current density. The current density is proportional to the current and inversely proportional to the beam length. The current density is also proportional to the number of particles in the bunch. The current density is proportional to the number of particles in the bunch and the beam length.

# DRAFT

## 4.1.1 Experimental Apparatus

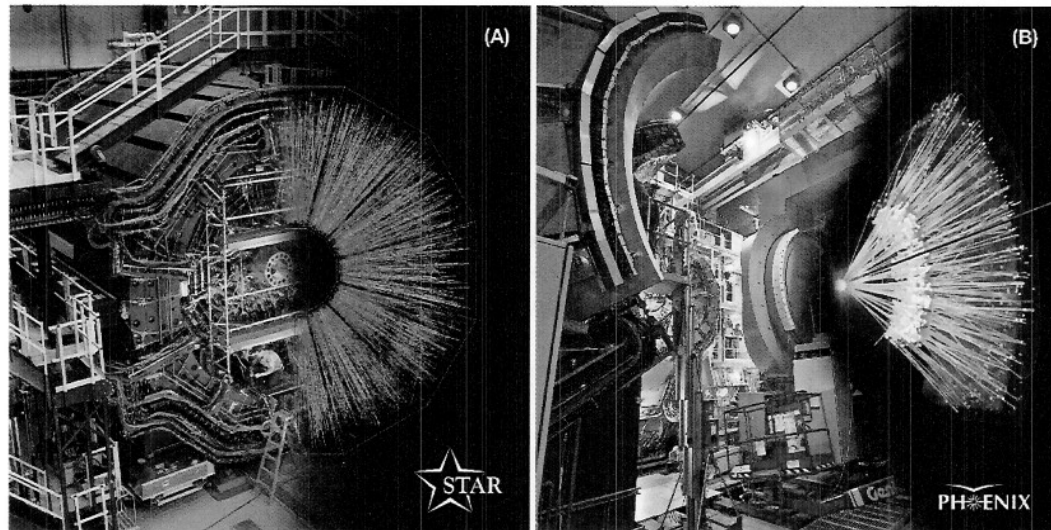


Figure 4.5: STAR (a) and PHENIX (b) with cutaways showing the event display for a heavy-ion collision as reconstructed by the detectors' electromagnetic calorimeters [51].

RHIC accelerates ions in a multi-stage process, summarized in Figure 4.1. The *beams* *start at* first stop is the **Electron Beam Ion Source**, built on top of a *200 MeV* linear accelerator (Linac). Once ions are injected into the Linac, they travel to the *Booster Synchrotron*. At this stage, ions are accelerated with pulsed RF fields. Once the beam of ions has been accelerated to nearly the speed of light, they are fed into the **Alternating Gradient Synchrotron** or AGS. At this time, ions are traveling at about  $0.37 c$ . By the time the ions leave the AGS, they are moving at  $0.997 c$ . Once the ions are ready, they are transferred to the **AGS-to-RHIC Line**, where a switching magnet pumps bunches of ions into either the counterclockwise circulating ring of RHIC, or the clockwise circulating ring of RHIC. The ions are *'spun-up'* here to maximum speed, and are accelerated around the RHIC complex - each beam-ion travels nearly *2.4 miles in microseconds*, for the duration of a physics-fill [52].

*Once, once once*

When the RHIC rings are filled with ions, the ions are bunched into rotating electromagnetic potentials called 'buckets'. There are 360 beam-buckets in total, but typically only a fraction are filled with ions. For this analysis, we took data with beams with 110 filled buckets. The sequence of beam buckets from one bunch to the next is referred to as a

*don't know what this means?*

*43  
not a very precise statement*

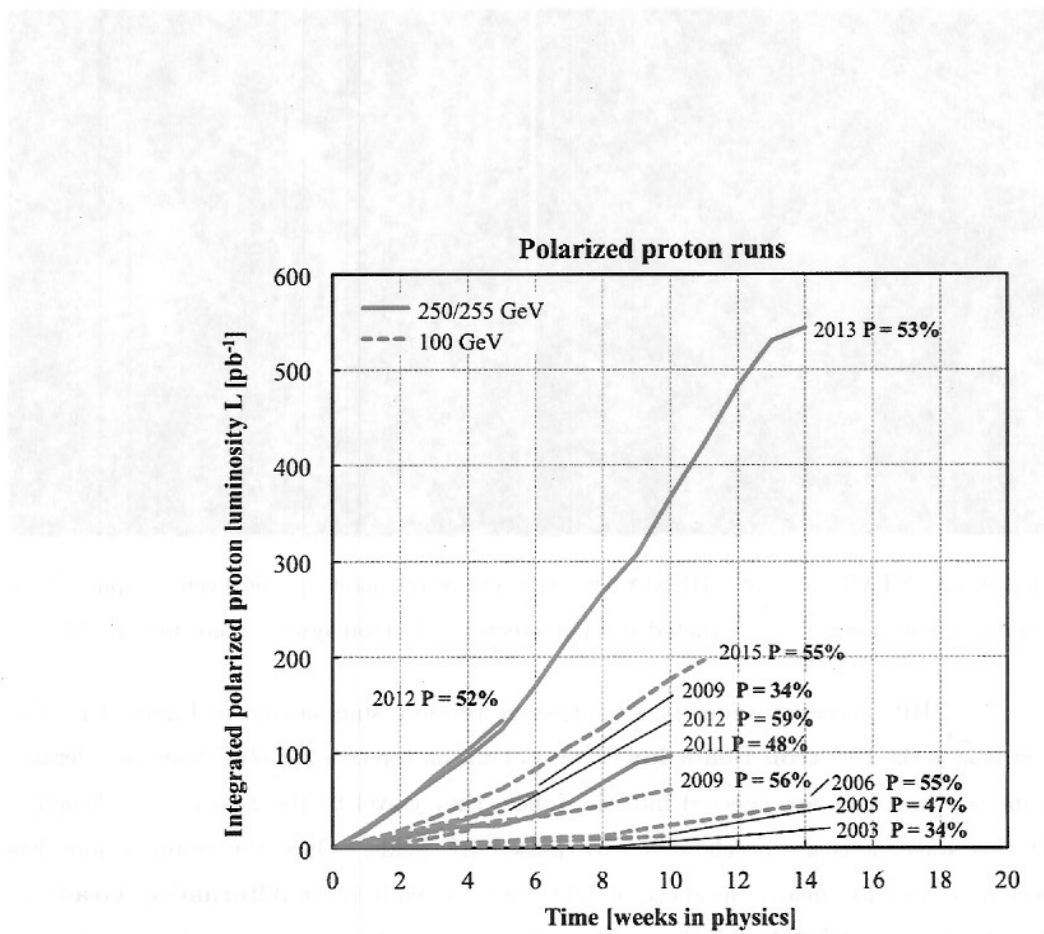


Figure 4.4: Upgrades to RHIC's electron lens have enabled massive improvements to luminosity - seen in the year 2013. The high luminosity was taken advantage of with an extra long proton+proton run. Figure obtained from [50]

# DRAFT

RHIC operating modes and total integrated luminosity delivered to 6 experiments					
Run	species	total particle energy [GeV/nucleon]	calendar time in physics	total delivered luminosity	average store polarization, (H-jet)*
<b>Run-7</b> CY2006/07, FY2006 18.4 cryo-weeks	$^{197}\text{Au}^{79+} + ^{197}\text{Au}^{79+}$	100.0	12.8 weeks	7.25 nb <sup>-1</sup>	—
	$^{197}\text{Au}^{79+} + ^{197}\text{Au}^{79+}$	4.6	3 shifts total, no continuous physics operation	small	—
<b>Run-8</b> CY2007/08, FY2008 19.0 cryo-weeks	$d + ^{197}\text{Au}^{79+}$	100.7 + 100.0	9.0 weeks	437 nb <sup>-1</sup>	—
	polarized p + p	100.2	3.4 weeks	38.4 pb <sup>-1</sup>	44%
<b>Run-9</b> CY2008/09, FY2009 22.0 cryo-weeks	$^{197}\text{Au}^{79+} + ^{197}\text{Au}^{79+}$	4.6	3 shifts	small	—
	polarized p + p	249.9	4.1 weeks	110 pb <sup>-1</sup>	34%
<b>Run-10</b> CY2009/10, FY2010 27.1 cryo-weeks	polarized p + p	100.2	9.9 weeks	114 pb <sup>-1</sup>	56%
	polarized pp2pp	100.2	3.5 days	0.6 nb <sup>-1</sup>	63%
<b>Run-11</b> CY2010/11, FY2011 24.4 cryo-weeks	$^{197}\text{Au}^{79+} + ^{197}\text{Au}^{79+}$	100.0	10.9 weeks	10.3 nb <sup>-1</sup>	—
	$^{197}\text{Au}^{79+} + ^{197}\text{Au}^{79+}$	31.2	2.9 weeks	544 $\mu\text{b}^{-1}$	—
<b>Run-12</b> CY2011/12, FY2012 22.9 cryo-weeks	$^{197}\text{Au}^{79+} + ^{197}\text{Au}^{79+}$	19.5	1.8 weeks	206 $\mu\text{b}^{-1}$	—
	$^{197}\text{Au}^{79+} + ^{197}\text{Au}^{79+}$	3.85	4.6 weeks	4.23 $\mu\text{b}^{-1}$	—
<b>Run-13</b> CY2012/13, FY2013 17.0 cryo-weeks	$^{197}\text{Au}^{79+} + ^{197}\text{Au}^{79+}$	5.75	1.4 weeks	7.8 $\mu\text{b}^{-1}$	—
	polarized p + p	249.9	9.7 weeks	166 pb <sup>-1</sup>	48%
<b>Run-11</b> CY2010/11, FY2011 24.4 cryo-weeks	$^{197}\text{Au}^{79+} + ^{197}\text{Au}^{79+}$	9.8	1.4 weeks	33.2 $\mu\text{b}^{-1}$	—
	$^{197}\text{Au}^{79+} + ^{197}\text{Au}^{79+}$	100.0	6.4 weeks	9.79 nb <sup>-1</sup>	—
<b>Run-12</b> CY2011/12, FY2012 22.9 cryo-weeks	$^{197}\text{Au}^{79+} + ^{197}\text{Au}^{79+}$	13.5	8 days	63.1 $\mu\text{b}^{-1}$	—
	polarized p + p	100.2	4.4 weeks	74.0 pb <sup>-1</sup>	59%
<b>Run-13</b> CY2012/13, FY2013 17.0 cryo-weeks	polarized p + p	254.9	4.9 weeks	283 pb <sup>-1</sup>	52%
	$^{238}\text{U}^{92+} + ^{238}\text{U}^{92+}$	96.4	3.1 weeks	736 $\mu\text{b}^{-1}$	—
<b>Run-13</b> CY2012/13, FY2013 17.0 cryo-weeks	$^{63}\text{Cu}^{29+} + ^{197}\text{Au}^{79+}$	99.9 + 100.0	5.4 weeks	27.0 nb <sup>-1</sup>	—
	polarized p + p	254.9	13.3 weeks	1.04 fb <sup>-1</sup>	53%

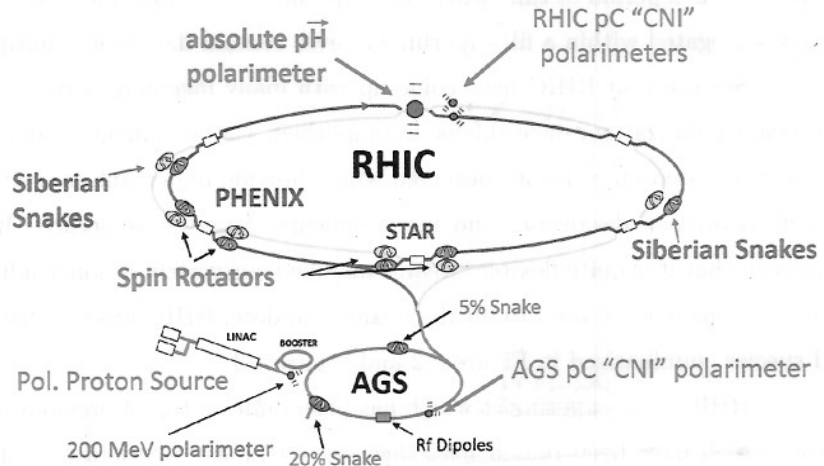
Figure 4.3: Though RHIC is currently still running (as of May 9, 2016), I include runs here up to and including the run producing my data set (Run 13). An unprecedented 13.3 cryo-weeks of running was awarded to the W-Physics group. Table produced from data posted at the RHIC run page [50].

# DRAFT

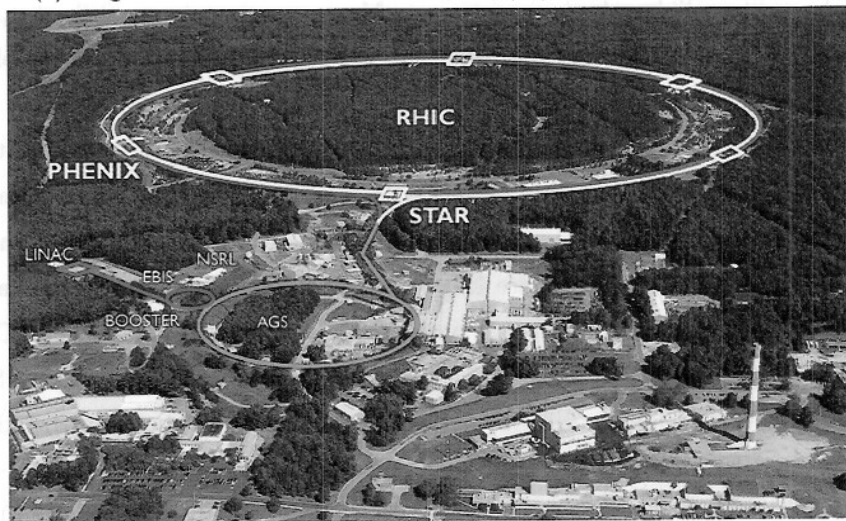
RHIC operating modes and total integrated luminosity delivered to 6 experiments						
Run	species	total particle energy [GeV/nucleon]	calendar time in physics	total delivered luminosity	average store polarization, (H-jet) <sup>*</sup>	
<b>Run-1</b> CY2000, FY2000 33.6 cryo-weeks	$^{197}\text{Au}^{79+} + ^{197}\text{Au}^{79+}$	27.9	3 shifts	< 0.001 $\mu\text{b}^{-1}$	—	
	$^{197}\text{Au}^{79+} + ^{197}\text{Au}^{79+}$	65.2	5.3 weeks	20 $\mu\text{b}^{-1}$	—	
<b>Run-2</b> CY2001/02, FY2001/02 40.7 cryo-weeks	$^{197}\text{Au}^{79+} + ^{197}\text{Au}^{79+}$	100.0	15.9 weeks	258 $\mu\text{b}^{-1}$	—	
	$^{197}\text{Au}^{79+} + ^{197}\text{Au}^{79+}$	9.8	2 shifts	0.4 $\mu\text{b}^{-1}$	—	
<b>Run-3</b> CY2002/03, FY2003 30.4 cryo-weeks	polarized p + p	100.2	8.3 weeks total, no continuous physics operation	1.4 pb <sup>-1</sup>	14%	
	d + $^{197}\text{Au}^{79+}$	100.7 + 100.0				
	polarized p + p	100.2		5.5 pb <sup>-1</sup>	34%	
<b>Run-4</b> CY2003/04, FY2004 26.7 cryo-weeks	$^{197}\text{Au}^{79+} + ^{197}\text{Au}^{79+}$	100.0	12.0 weeks	3.53 nb <sup>-1</sup>	—	
	$^{197}\text{Au}^{79+} + ^{197}\text{Au}^{79+}$	31.2	9 days	67 $\mu\text{b}^{-1}$	—	
	polarized p + p	100.2	6.1 weeks total, no continuous physics operation	7.1 pb <sup>-1</sup>	46%	
<b>Run-5</b> CY2004/05, FY2005 31.4 cryo-weeks	$^{63}\text{Cu}^{29+} + ^{63}\text{Cu}^{29+}$	100.0		42.1 nb <sup>-1</sup>	—	
	$^{63}\text{Cu}^{29+} + ^{63}\text{Cu}^{29+}$	31.2	12 days	1.5 nb <sup>-1</sup>	—	
	$^{63}\text{Cu}^{29+} + ^{63}\text{Cu}^{29+}$	11.2	5 shifts	0.02 nb <sup>-1</sup>	—	
	polarized p + p	100.2	9.4 weeks	29.5 pb <sup>-1</sup>	47%	
	polarized p + p	204.9	2 stores	0.1 pb <sup>-1</sup>	30%	
<b>Run-6</b> CY2006, FY2006 21.2 cryo-weeks	polarized p + p	100.2	13.1 weeks	88.6 pb <sup>-1</sup>	55%	
	polarized p + p	31.2	12 days	1.05 pb <sup>-1</sup>	50%	

Figure 4.2: Runs 1 - 3 at RHIC focused on commissioning work for experiments measuring collisions at RHIC. Work was mostly characterized by heavy-ion measurements related to understanding Quark-Gluon Plasma. The spin program began with Run 5. Table produced from data posted at the RHIC run page [50].

# DRAFT



(a) Diagram of RHIC Accelerator Complex, (Figure from Kiyoshi Tanida)



(b) Aerial photograph of RHIC Complex [49]

Figure 4.1: A diagram of the acceleration process of RHIC is shown in the top panel, and an aerial view is on bottom. RHIC is nearly four miles in circumference and collides a variety of ions at center-of-mass energies between  $62\text{GeV}$  and  $510\text{GeV}$ .

*Shawn on the  
bottom part*

39

*not italic  
add a short space: 62.41, GeV  
actually 5.2 cm ~ something*

# DRAFT

where a run is a period of time where the experiment is taking data. At PHENIX, runs are always segregated within a fill - no run will ever contain data from multiple fills.

Scientists at RHIC have come up with many ingenious ways to create and maintain beam polarization, once this is accomplished, various kinematically select probes are engineered, based on collisions observed which provide important cross-checks to DIS data as well as original discoveries and measurements of proton structure. RHIC is a unique collider in that it is quite flexible. Beams may be transversely or longitudinally polarized, a variety of ions may be used to fill the beams. To date, RHIC has collided many beam ions and species, summarized in Figure 4.2 and Figure 4.3.

RHIC is an ~~facility~~ experiment which has been built on top of previous accelerator experiments which have been reused magnificently - a Linear Accelerator, a booster ring, and ~~the~~ an Alternating Gradient Synchrotron, all of which now have been repurposed to create ~~a~~ the necessary high-quality collider physics experiment. Many experiments are still set up around various egress points along the acceleration chain, which are publicised on the Brookhaven National Laboratory website [www.bnl.gov](http://www.bnl.gov)

At the time of writing of this thesis (Spring of 2016), there are two experiments which are actively taking data from collisions produced by RHIC: The Pioneering High Energy Nuclear Interaction Experiment (PHENIX, Section 4.4, Figure 4.5), and the Solenoidal Tracker at RHIC (STAR, Figure 4.5). STAR and PHENIX are complimentary to each other - PHENIX has a very high precision centrally covering Electromagnetic Calorimeter, and other high precision detectors, but lacks full kinematic coverage, whereas STAR has lower precision, but has nearly full kinematic coverage around the beam intersection at its center.

RHIC's luminosity and beam polarization has been continuously improving (Figure 4.4) since RHIC was first turned on. As we will discuss later (4.5), this increased luminosity observed in 2013, was maximally leveraged with upgrades to the PHENIX detector.

# DRAFT

## Chapter 4

# The Relativistic Heavy Ion Collider

### 4.1 Overview

While there have been many experiments which have performed deep inelastic scattering over the years, the experiments built around the Relativistic Heavy Ion Collider at Brookhaven National Laboratory are positioned to take advantage of the unique accelerator.

The Relativistic Heavy Ion Collider (RHIC) is the world's only intersecting ring particle accelerator which is capable of producing polarized proton beams. The beams are differentiated with the mnemonic "Blue" and "Yellow" beam. The Blue beam circulates clockwise when viewed from above the RHIC complex, the Yellow beam circulates counter-clockwise. As is typical for intersecting ring experiments, the beams are bunched, with bunches of ions intersecting at designated intersection points, around which experiments are built. The Blue beam is nominally used to time these collisions, such that experiments which have bunch-sensitive measurements (i.e. any experiment where bunch polarization is important) can associate the correct bunch polarization with the correct collision. This will be discussed more in the section of beam-polarization (4.3).

RHIC generally separates data taking into beam 'fills' which are uniquely numbered, and for which general data characterizing the machine state is logged in various databases and online logbooks. Each fill is a unique population of beam ions, circulating around the RHIC rings. The beam ions are subdivided into discrete collections of ions called bunches. At the end of each fill, (typically 8 hours of collisions), the beam is dumped, and a new fill is generated. Experiments built around RHIC generally subdivide fills into 'runs',

# DRAFT

## 3.5 Cross Sections and Luminosity

- vernier analysis note intro, equations
- summarize the papers on Lumoninosity

## 2.2.5 Early Particle Physics and The Eightfold Way

The hydrogen atom, and its spectra was well modeled with quantum mechanics by the end of early 20th century, however attempts to study Helium were not as successful. However, in 1932, when Chadwick turned a beam of helium particles (at that time only known as  $\alpha$  particles) on a sample of Beryllium, he observed that neutral, non-ionizing, penetrating radiation was produced [29]. Photons were ruled out as possible candidates, leading to the discovery of the neutron. Protons and neutrons were hypothesized by Heisenberg to both be the same state of a new conceptual particle, the nucleon, [30]. In the same year, Anderson discovered the positron.

By 1934, Hideki Yukawa (Fig. 2.9) had created an effective field theory for interactions of 'elementary particles' (at this time, thought to be protons and neutrons). He predicted the existence of mesons, and wrote down an effective field theory which described how protons and neutrons bind together in the nucleus [31].

Though non-relativistic quantum mechanics was mostly complete by 1934, scientists were already hard at work incorporating relativistic corrections to the theory. Experiments with cosmic rays soon revealed the existence of muons and the first observation of mesons.

Three separate paths eventually lead to the development of particle accelerators, which are to date, the best mechanism we possess in physics to probe nuclear structure. These accelerators are an outgrowth of ever more intense Rutherford-style experiments, Tandem Van-Der-Graaf generators, resonant acceleration techniques, RF linacs, and betatron accelerators [33].

By the 1950's, a cornucopia of strange new particles had been discovered, both matter and antimatter. But scientists drove forward, deeper, yearning to discover what was fundamental. By the 50's, neutrinos had been proposed, as well as Kaons, Pions, and Lambdas. Physicists were doing nuclear chemistry, in a sense, attempting to work out how quickly some particles decayed, and what decays were allowed or forbidden - science entered an age of nuclear alchemy.

"Strange" particles were discovered ( $K$  and  $\Lambda$ ), so called because in bevatron experiments, they were produced in great quantities, but were slow to decay, unlike the faster  $\pi$  decay. Gell-Mann proposed that this strangeness in matter was due to a new quantum number (he called it 'strangeness'). The name stuck. [34], [35], [29]

# DRAFT

these particles, which were important for making precise predictions for atomic spectra [27].

By this time, the proton was already known to reside in the enigmatic nucleus of atoms, however, attempts to use Quantum Electrodynamics to describe the state of the nucleus failed - it was clear that there was a very strong force, holding together the protons of a nucleus tightly - far in excess of the electromagnetic repulsion felt by the positively charged particles. There was a completely different coupling strength between this apparent strong nuclear force, and the better known electromagnetic coupling. Further complicating an understanding of the nucleus is the fact that as the length scale of probing decreases, the energies probed increase, fundamentally making the nucleus a relativistic object. Experimental physics would once again, forge ahead, in attempting to understand the inner workings of the nucleus, in the time-honored tradition of performing scattering experiments.

The first major breakthrough in this field came from the work of Werner Heisenberg, Hans Bethe, and Enrico Fermi, who developed the theory of quantum mechanics in the early 1930's. This theory provided a framework for understanding the behavior of subatomic particles, and paved the way for the development of nuclear physics. In particular, the theory of quantum mechanics allowed for the prediction of the existence of the neutron, which was later confirmed experimentally by James Chadwick in 1932. The discovery of the neutron led to the development of nuclear fission, which has had a profound impact on modern society. The theory of quantum mechanics also provided the foundation for the development of the atomic bomb, which was used in the bombing of Hiroshima and Nagasaki during World War II. The development of nuclear fission and the atomic bomb has had a significant impact on the world, and continues to be a topic of interest and concern today. The theory of quantum mechanics has also had a profound impact on the development of modern technology, such as computers and mobile phones. The principles of quantum mechanics have been applied to a wide range of fields, including chemistry, materials science, and medicine. The theory of quantum mechanics has revolutionized our understanding of the fundamental nature of matter and energy, and continues to be a source of inspiration and discovery for scientists and engineers around the world.

# DRAFT

of matter - both wave-like, and particle like. The notion that probing the structure of matter did not yield a simple, deterministic hierarchy of structure was revolutionary, confusing, and bizarre, and still is to this day.

It was found that not only light possesses this wave-particle duality, but also the very particles that make up atoms as well. These models were formalized by Dirac, Hilbert and Von-Neumann.

Though experiment tended to lead theory, regarding understanding the composition and rules of interactions in matter, in the mid 20th century, further refinements and additions to quantum mechanics gave birth to quantum field theory. While early quantum models were very successful at describing static particles trapped in static potentials - such as refining atomic theory to include predictions of observed atomic spectra, more work was needed to understand the relationship between electrical currents, light and magnetism. These concepts were all related by Maxwell [26] in the latter half of the 19th century, but did not make good predictions for systems in motion.

Dirac was first to create a model for describing the electron, its behavior in electromagnetic fields, and photon emission and absorption, under fully relativistic and quantum conditions [27]. Dirac's model was so successful, that it would become the basis for what we now call quantum electrodynamics. Much of the mathematical formalism has been reused to describe other field theories, which are the ultimate language which model and describe the structure of matter - including the insides of a proton.



(a) Paul Dirac, 1933 [28]

$$\left( \beta mc^2 + c \left( \sum_{n=1}^3 \alpha_n p_n \right) \right) \psi(x, t) = i\hbar \frac{\partial \psi(x, t)}{\partial t} \quad (2.1)$$

(b) The Dirac Equation

$\Box \psi = 0$

Figure 2.8: Paul Dirac, next to his original formulation of the Dirac Equation, describing the wave function for an electron with rest-mass  $m$ , in terms of its spacetime coordinates.

Dirac's work also began to incorporate relativistic effects in his wave equations modeling the electron, as well as crucially incorporating the spin (I.e. Dirac Spinors) of

# DRAFT



Figure 2.7: The attendees of the Solvay Conference in Brussels, 1927 [25].

## 2.2.4 Early Quantum Theory

During Rutherford's time, experiments were already underway which were investigating modeling light as a wave phenomena. This was in contrast to Newton's (unverified) corpuscular theory of light. The argument whether light was wave-like or particle-like eventually lead to a classical field theory describing light, and the electromagnetic interaction, yet scientists such as Max Planck were proposing theories which required the quantization of light [24]. Einstein would show that in his analysis of the photoelectric effect, that light indeed was quantized into 'corpuscles'. The nascent atomic theory of matter was also hinting at a hidden, quantized world.

At the Solvay Conference in Brussels, Figure 2.7, in 1927, we saw an unprecedented gathering of some of the most important figures in modern physics, all in one place, laying down the foundations of what would become quantum mechanics. These scientists defined the nature and rules of quantum mechanics - the weird model which accommodates a duality

# DRAFT

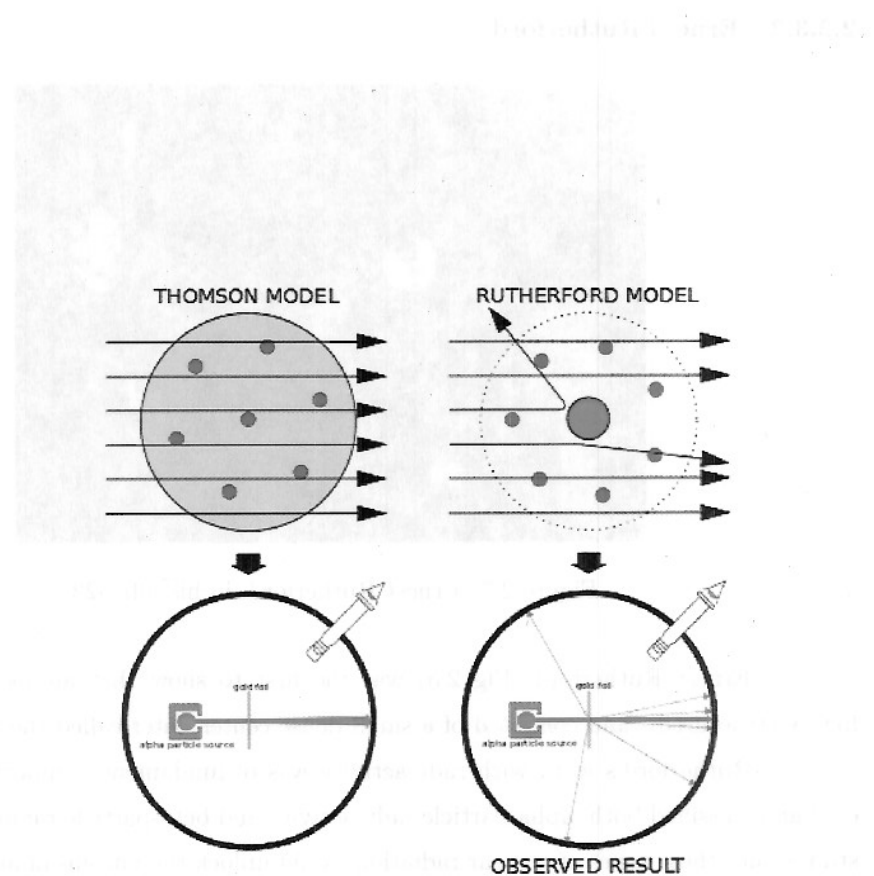


Figure 2.6: Ernest Rutherford’s historic experiment, showing (top right) that atoms were composed of a small dense nucleus, in contrast to Thomson’s ‘pudding model’ of homogeneous charge (top left). The experiment, (bottom left and right) contrast the expected results (bottom left) against the observed results (bottom right) [23].

# DRAFT

## 2.2.3.3 Ernest Rutherford

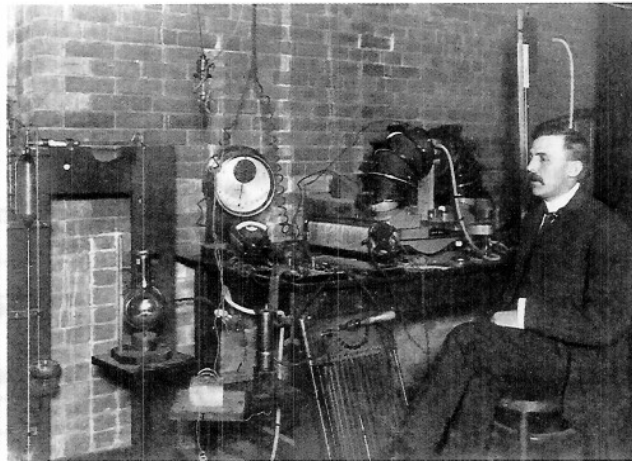


Figure 2.5: Ernest Rutherford, in his lab. [22]

Ernest Rutherford (Fig 2.5) was the first to show that atoms themselves were highly structured - and consisted of a small dense center, later called the nucleus.

Rutherford's work with radioactivity was of fundamental importance, he discovered and classified both alpha-particle radioactivity and beta-particle radioactivity. Further studies into these types of nuclear radiation would unlock the nucleus of atoms through the work of future scientists. Notably, Rutherford discovered the proton.

Rutherford's proposed planetary model for the nucleus, while technically wrong, shifted paradigms from the pudding model of atoms, to the more familiar nucleus + electron cloud model which has been spectacularly modeled and verified with the forthcoming scientists which defined the field of quantum mechanics.

Rutherford's work helped push us out of the cocoon of classical mechanics into the weird world of the quantum mechanics - scientists would soon find that the nucleus is not just a dense concentration of charge, but a probabilistic structure, with rich sub nuclear structure.

# DRAFT

### 2.2.3.1 John Dalton

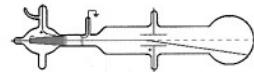
While many had postulated the existence of atoms, the first evidence based theory which suggested the existence of atoms was produced by John Dalton in the early 19th century. Dalton made an important conceptual leap to relate the existence of stoichiometric ratios in chemistry to the presence of small, individual functional units in his experiments with chemical reactions. Dalton's realization was only made possible due to his careful accounting of reactants in his experiments.

It was not until Einstein's 1905 theory on Brownian Motion was experimentally verified by Jean Perrin to place limits on the mass and size of atoms that Dalton's atomic theory was ultimately vindicated [18].

### 2.2.3.2 J.J. Thompson



(a) J.J. Thomson [19]



(b) Cathode Ray Tube [20]

Figure 2.4: Left: J.J. Thomson, who showed that cathode ray tubes were in fact producing the first observed subatomic particle: the electron. Right: A cartoon of Thomson's cathode ray tube setup. Electrons would be deflected by a magnetic field, sent from cathode to anode.

Thomson (Figure 2.4) would discover that atoms are not the smallest, indivisible piece of matter. In his landmark experiment, he used cathode ray scattering experiments to show that cathode rays were in fact subatomic particles. He showed these cathode rays were identical to particles given off by the photoelectric effect, and that these same particles were responsible for electric current. He had discovered the electron. And, if atoms were not the smallest piece of matter, then perhaps, atoms themselves might not be "indivisible" as previously thought [21].

# DRAFT

## 2.2.3 Atomic Theory

On the shoulders of giants such as Newton and Galileo, science finally came to know the tool which has been indispensable to modern particle physics: scattering. Rutherford and Thompson both carried out the most important scattering experiments in modern science, and provided us with the first hints of a hidden, quantum world, though it would not be until the 20th century that these important experiments would be fully contextualized with a theory of quantum scattering.

Scattering experiments offer a very powerful method where we one uses a well known initial state of matter (typically in the form of a beam), allows this beam to interact with an unknown configuration of matter, and measures the scattered beam. By carefully studying the kinematics of the scattered beam, we can create models which allow us to understand the structure of the target matter or describe the nature of the interaction between the beam and target.

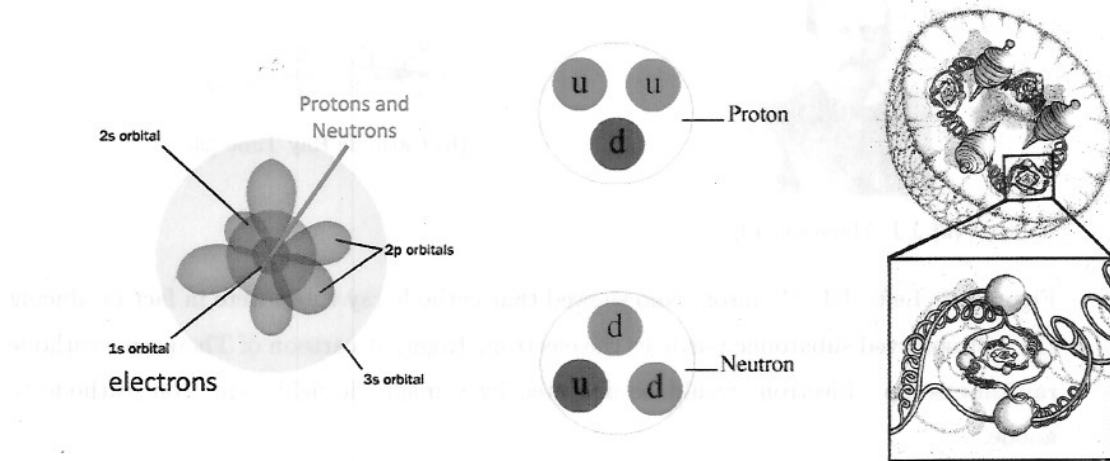


Figure 2.3: As we journey down further in scale, matter begins to look quite different. In fact, the models we use are scale dependent. Thomson 2.8, and Rutherford 2.5 began to see matter as collections of atoms (left) [15] (though not in terms of the orbital structure pictured), though it would not be until 20th century quantum mechanics that electron orbitals were discovered. Soon, nuclei were discovered to be divisible into protons and neutrons [16] (center), which in turn were discovered to be composed of a sea of quarks and gluons (right). (Right image drawn by the talented Astrid Morreale, PhD, [17]) Just reference it

# DRAFT

## 2.2.2.2 Isaac Newton

Fittingly born in the same year as Galileo's death, Isaac Newton would carry on Galileo's legacy of rigorous mathematical modeling mixed with experimentation. Perhaps no other scientist has touched so many different aspects of physics, from theories of propagation of light, to celestial mechanics, to mathematics, and kinematics.

Newton's Principia is perhaps the most important scientific work ever published. It opened the doors of the universe in a way that nobody has since duplicated. Newton's laws of motion are still taught in school today, and although they have since been shown to be inaccurate at the smallest and largest scales, they still provide startlingly accurate predictions for the regular motion of matter.

One particularly tantalizing theory of Newton's was the corpuscular theory of light. Although not his most influential theory by far, the idea that an apparently continuous medium such as a beam of light might be made of small packets of energy (corpuscles) turned out to be partially right [14].

Newton's theories, and contributions to science are enormous, and have moved us deeper still into the underpinnings of matter. It would not be until roughly 200 years after his death, in the 19th century, that we finally can take the first steps into the world of the atomic, and sub-atomic: the world of the proton.

# DRAFT

## 2.2.2 The Scientific Revolution

Thanks to the mathematical foundations laid out, build, and maintained by the minds of the Islamic Golden Age, Europe was well poised to reignite the flames of scientific inquiry, during the post Renaissance Scientific Revolution [10].

This period of growth in science was unprecedented during the Scientific Revolution, thanks to the seeds of empiricism germinated during the Islamic Golden Age, fertilized by the Italian Renaissance, and helped to flourish through British Empiricism [11].



(a) Galileo [12]



(b) Newton

Figure 2.2: Giants in the age of Empiricism, Newton (left) and Galileo (right) both made foundational contributions to Physics. Galileo lived in Italy, born in 1564 and dying in 1642. Newton lived in England from 1642 until his death in 1727

### 2.2.2.1 Galileo Galilei

While Galileo is best known for his work in Observational Astronomy, his importance to science extends beyond this. During his years in exile for his controversial views of the heliocentric universe, he produced some of his most important scientific work in kinematics [13]. What made this work remarkable is the care that Galileo took in merging careful mathematical modeling with well designed experimentation. This methodical approach to inquiry laid the foundation for others to slowly begin to pull back the curtains obscuring physical law.

Galileo's formalization of the scientific method inexorably set science on a course to delving deep into the nature of matter, and the laws of nature.

# DRAFT

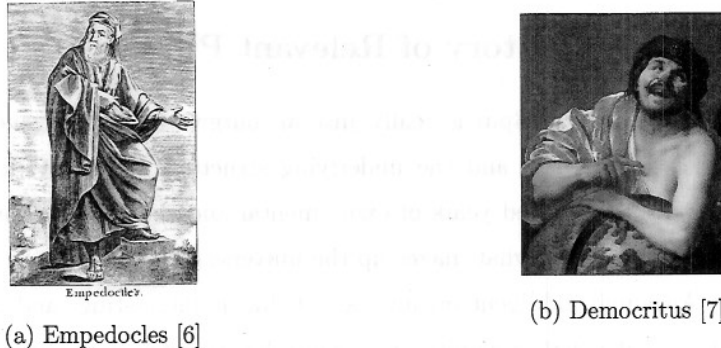


Figure 2.1: Two Greek philosophers, who made important philosophical contributions our understanding of matter. Empedocles (left), postulated the precursor to the elemental theory of matter[8] and Democritus (right), postulated the precursor to the atomic theory of matter.

substances' was an important step forward. Proto-scientists were beginning to generate models which derived our complicated observations, from simpler forms.

It took centuries of cultivation, leading up to the Scientific Revolution, for the next great steps to occur, for science. Thankfully; the luminaries of the Islamic Golden Age kept the fires of inquiry burning [10].

# DRAFT

## 2.2 A Brief History of Relevant Physics

The study of Spin is really just an outgrowth of the general study of matter. Our models for matter, and the underlying structure of matter (in the modern sense), represents over a hundred years of experimental and theoretical efforts, and thousands of years of contemplating what makes up the universe.

Although indulgent on my part, I find it interesting, and humbling, to try and map out the path that humanity and science has trodden on its way to understanding the building blocks of the universe. To find the first time that humanity had murmurings that suggested our visible world is built from invisible, fundamental building blocks, we must travel back, nearly 2,500 years into the past.

Rather than provide a complete mathematical background to my measurement from a historic perspective, I will instead focus on the experimental historic narrative surrounding our quest to understand the structure of matter. After, I will present mathematical formalism relevant to this measurement directly - if the reader desires an exhaustive mathematical context, I invite them to read the classic tomes on Field Theory by Weinberg and reference the numerous theses written by my colleagues in theoretical physics and phenomenology.

### 2.2.1 Ancient Foundations

Sometime around 490 - 370 BCE lived two philosophers, Empedocles (Fig 2.1a), and Democritus (Fig 2.1b). Both men lived approximately at the same time, and made huge philosophical leaps in attempting to understand the nature of the visible world.

Democritus was part of a movement of thought which was first to make the intellectual jump that perhaps matter was not a continuum, but instead, composed of 'atomon', small, indivisible particles which when configured together, created all that is observable [9]. Empedocles was making equally important philosophical strides - in a manner complimentary to Democritus' opinion that matter must be made of atomon, Empedocles argued that matter is composed of elemental primitives [8].

Although Empedocles' 'periodic table' was only composed of Earth, Water, Fire, and Air, the idea that some unseen transmutation of elemental forces might generate observables in nature with quite different (but perhaps reminiscent) properties then the 'pure'

# DRAFT

the world as we know would collapse on itself, making any kind of extended non-exotic structures which currently exist by virtue of the Pauli exclusion principal, impossible.

It is also important to note that the *Standard Model* is not the only theory of particle physics. There are other theories such as supersymmetry, string theory, and M-theory which attempt to describe the fundamental particles and their interactions. These theories often involve additional dimensions or fields that are not yet experimentally confirmed. However, they provide alternative frameworks for understanding the fundamental laws of nature.

The Standard Model is based on the idea that all matter is composed of fermions, which are particles that obey the Pauli exclusion principle. This means that no two fermions can occupy the same quantum state at the same time. Fermions include electrons, protons, neutrons, and quarks. They have half-integer spin and interact via the strong nuclear force. Fermions are also subject to the weak nuclear force and electromagnetism. The Standard Model also includes bosons, which are particles that do not obey the Pauli exclusion principle. Bosons include photons, gluons, and W and Z bosons. They have integer spin and interact via the electromagnetic force and the weak nuclear force. The Standard Model is a very successful theory, but it does not account for all aspects of particle physics. For example, it does not include gravity, which is a fundamental force in the real world. Gravity is described by general relativity, which is a theory of gravitation developed by Albert Einstein. General relativity describes gravity as a curvature of spacetime caused by mass and energy. It is a very accurate theory for large-scale phenomena, but it becomes less accurate at small scales. At small scales, the Standard Model and general relativity do not agree. This is where string theory and M-theory come in. These theories attempt to unify the fundamental forces of nature into a single framework. They propose that the fundamental particles are not point-like, but rather are tiny loops or strings. These strings vibrate at different frequencies and produce different particles. The strings are embedded in a higher-dimensional space-time, which is curved by the presence of mass and energy. This provides a unified theory of everything, including gravity. However, these theories are still not fully confirmed by experiment. They require very high-energy collisions to test their predictions, which are difficult to achieve. Nevertheless, they provide a fascinating framework for understanding the fundamental laws of nature.

# DRAFT

## Chapter 2

# Historic Perspective on the Structure of Matter and Spin

*phenomenon?*

### 2.1 The Phenomena of Spin

Spin is a fundamental quantity possessed by all elementary particles. We use the word 'spin' to describe the property, because particles which possess spin, behave as though they have some kind of intrinsic, hidden rotation, as if they were 'spinning'. The dimension of spin, therefore is angular momentum. What is somewhat bizarre about spin, is that we do not observe anything physically spinning - although there are some phenomena (such as orbital angular momenta) which can be naively thought of as a 'spinning system' (but this description escapes classical analogy, due to its quantum, probabilistic nature). The role of Spin in Physics is of foundational importance, and yet, we have not successfully produced a model which can accurately predict the spin of hadrons. *do you mean spin makes up the spin of a particular hadon?*

The presence of spin in relativistic particles creates the phenomena of chirality, which has huge implications for how elementary particles can generate structure in matter itself [5]. In the case of the weak interaction, the presence of spin, which creates Chiral spinors breaks the left-right symmetry of weak coupling in matter (a fact which will be exploited in this thesis to probe the spin of the proton sea).

The phenomena of spin also changes the rules for how ensembles of particles may exist in a potential. Particles with spin are fermions, and because these particles must obey Fermi-statistics, we can observe structure in matter in the universe. Without spin,

# DRAFT

will be discussed

*second part*  
The other portion of this thesis will discuss the Vernier Analysis, which is instrumental for every single-cross-section calculation taken with RHIC data. The thrust of the Vernier Analysis is to determine the beam luminosity at PHENIX's interaction point, so *the objective* *enables one* *as to normalize these cross-section calculations.* This is done with a series of specialized Vernier-Scans, where beams are scanned across one-another in order to measure beam geometry. The luminosity can then be calculated from first principals, and compared to the advertised machine luminosity published by RHIC's collider-accelerator department. I began working with the Vernier Analysis under the tutelage of K. Oleg Eyser, but eventually moved to work independently on the analysis, producing an entire software framework for handling data cleaning, analysis, visualization and simulation.

*not here...* } As an additional note, while I attempt to be consistent with my notation, my convention, when pulling mathematics from cited sources, is to keep the source mathematical notation. Additionally, for other sections, when I reproduce definitions or calculations which are perhaps more related to general PHENIX analyses, I will attempt to emulate the notational style found in Hideyuki Oide's thesis ( ??), which has served as a seminal document for guiding this analysis, as well as the Run 12 analysis.

*right with the author and his paper* }  
In addition to the main analysis presented in this thesis, there are several other analyses which have been performed with the Vernier Analysis. These include the calculation of the beam luminosity, the calculation of the beam energy loss, and the calculation of the beam energy loss per unit length. These analyses are based on the same underlying principles as the main analysis, but they are designed to be used in different contexts. For example, the beam energy loss analysis is used to calculate the energy loss of a beam as it passes through a medium, such as a detector. The beam energy loss per unit length analysis is used to calculate the energy loss of a beam as it passes through a medium, such as a detector, over a given distance. These analyses are useful for understanding the behavior of beams in different environments, and for calculating the energy loss of beams in different environments.

# DRAFT

of physicists, we have magnificently described this important particle, and understood much of its properties. However, one property which still defies our descriptions is its fundamental angular momentum, spin.

*back tick*

Our understanding of the proton has evolved and sharpened since the first experiments in deep inelastic scattering showed that the proton is not a fundamental particle [2]. Gell-Mann later planted the seeds of a theoretical framework which could in part describe some of the structure of baryons, a class of hadrons which we may naively describe as composed of three 'valence quarks' [3]. We can apply well known spin-sum rules to the individual spins of the valence quarks which compose the proton in our naïve valence-model to produce a correct prediction for the protons' spin  $\frac{1}{2}$ . When experimenters set out to measure the contribution of these valence quarks in 1988 at the EMC experiment [1], they were flabbergasted to find that the valence quarks carry only a small fraction of the proton's spin. Although recent papers [4] suggest that this 'spin crisis' is simple due to mis-attribution of spin, most literature to date has focused on understanding how to model the proton with parton distribution functions. These parton distribution functions come in many varieties, and probe different degrees of freedom within the proton, in both the case of unpolarized parton distribution functions, and polarized parton distribution functions.

*not scientific*

→ Some picture illustrates "spin crisis"

## 1.2 Scope and Objectives of This Work

This thesis will describe the research I carried out between May of 2010 through August of 2016. I will often quote work that was carried out in active collaboration with Ralf Seidel, Francesca Giordano, Daniel Jumper, Sanghwa Park, Abraham Meles and Chong Kim. Daniel, Abraham, Ralf, Francesca, and myself all worked on the 2013 polarized proton data set taken at RHIC with PHENIX. This analysis comprises the body of work devoted to calculating  $A_L$  for the  $W \rightarrow \mu$  decay. Since 2013, the five of us collaborated closely on all aspects of the work, which provided invaluable cross-checks at nearly every stage. Many of the figures in this document were produced by our collective efforts, and I will do my best to cite when possible, if one analyzer played a particularly large role in generating the data or visualization, however after several years of working together, I will certainly fail to attribute, or mis-attribute at times.

*should be in  
"acknowledgments"  
It's your thesis...*

In the flat part of this Thesis...

# DRAFT

This document is a draft of my thesis. It contains many errors, typos, and other mistakes. It is not intended for publication or distribution outside the author's immediate family or friends. It is a work in progress, and I welcome any comments, suggestions, or criticisms. Please do not cite this document without the author's permission. Thank you.

## Chapter 1

### Introduction

THIS THESIS IS CURRENTLY AN UNPUBLISHED DRAFT. IT HAS NOT BEEN SUBMITTED AND MAY HAVE MISSING CITATIONS AND CONTENT

A brief note - figures used here *without* attribution were either: produced by me, produced in collaboration with others in my working group, or obtained from authors who labeled them for reuse without attribution. I have taken great pains to cite all figures, tables, and content; even if taken from a source which does not require attribution. Happily, any work undertaken in the United States that is the beneficiary of Federal funding is *automatically* public domain, and may be reused *without attribution*. This naturally includes work produced by any experiment receiving DOE funding. Of course, anyone who makes a habit of reusing another's hard work under the protection of this particular facet of copyright law, might want to carefully reflect on the various ways of translating '*teste di cazzo*' from Italian to English.

#### 1.1 A Brief History of the Proton

The angular momentum of the proton and neutron has been a subject of study for the last 30 years. One of the challenges of particle physics is to create a framework which can accurately describe matter, as well as predict the behavior of matter at all energy scales. Protons and neutrons are baryons which make up the majority of the mass in the visible universe, yet fully understanding the origins of their properties - such as mass and spin, still eludes us. However, through the application of the scientific method over many generations

# DRAFT

6.2	Simulated sub processes in Run 13 including their generated event numbers as well as the corresponding luminosity and cross sections. Dr. Sanghwa Park has done an extensive analysis of the simulated data to determine an appropriate k-factor. Process which contribute very little to the muon background include W had, W tau, and $d\gamma$ ; they are scaled to zero. . . . .	100
6.3	$\eta$ dependent trigger efficiencies are calculated for the South arm in 20 $\eta$ bins. Each correction has both systematic and statistical error accounted for. . . . .	102
6.4	$\eta$ dependent trigger efficiencies are calculated for the North arm in 20 $\eta$ bins. Each correction has both systematic and statistical error accounted for. . . . .	103
6.5	South arm $W \rightarrow \mu^-$ fit results per analyzer [70] . . . . .	133
6.6	A summary table from the results of the EULMF to the unbinned data set, summed to one $\eta$ bin per arm and charge. . . . .	135
7.1	Patters P1-P8 were filled into RHIC for the first portion of the 2013 data taking period, with P21-P28 being filling in the second portion. For each pattern, from left to right, bunch 0 in the blue or yellow beam is filled with the leftmost polarization, with bunch 1 getting the next, and so on. The pattern repeats as soon as the end has been reached, until we get to the last filled bunch, with any empty bunch being 'polarized' as if it were not empty. . . . .	144
7.2	Due to much higher integrated luminosity of Run 13, we can actually subdivide the muon yields into rapidity bins for the purposes of trying to cover a wider kinematic range (at the expense of uncertainty). Here, we see the South arm's yields for each helicity combination of colliding protons, with the polarization of the blue beam and yellow beams color coded in column 2. Recall that of the yields, about 20% are actual signal events. . . . .	146
7.3	Due to much higher integrated luminosity of Run 13, we can actually subdivide the muon yields into rapidity bins for the purposes of trying to cover a wider kinematic range (at the expense of uncertainty). Here, we see the North arm's yields for each helicity combination of colliding protons, with the polarization of the blue beam and yellow beams color coded in column 2. Recall that of the yields, about 20% are actual signal events. . . . .	147
7.4	As a consistency check to previous analysis which only had enough statistics for two $\eta$ bins, one forward, and one backward for $A_L^{W+}$ , we have binned the data to match. Here, we see a division of the data by arm, charge, and helicity combination, which is color-coded for the polarization of the blue and yellow beams. Note that of the yields, only $\sim 20\%$ of the yield comes from a W-Boson decay. . . . .	148
7.5	A summary of the sign convention when we consider rapidity with respect to the probe beam, as opposed to the rapidity of the PHENIX coordinate system. . . . .	150